A Low-Complexity Modified Pilot-Based Channel Estimation Method for IEEE 802.22 Systems with Performance–Efficiency Trade-off

Kaushik Das, D. Sagar Babu, Chetna Singhal, Amit Kumar Dutta, Raja Datta

A Low-Complexity Modified Pilot-Based Channel Estimation Method for IEEE 802.22 Systems with Performance–Efficiency Trade-off

Kaushik Das[1], D.Sagar Babu[1], Chetna Singhal[3], Amit Kumar Dutta[2], Raja Datta[1]

[1]Department of Electronics and Electrical Communication Engineering,
[2]G S Sanyal School of Telecommunication,
Indian Institute of Technology, Kharagpur–721302, India
[3]Inria, Univ Rennes, CNRS, IRISA, Rennes, France
E-mail: kaushikforresearch@gmail.com, sagarduripalli7777@gmail.com,
chetna.singhal@inria.fr, amitdutta@gssst.iitkgp.ac.in, rajadatta@ece.iitkgp.ac.in

Abstract—
Wide-area cognitive *orthogonal frequency-division multiplexing* (OFDM) links in *television white space* (TVWS) under the *IEEE 802.22 Wireless Regional Area Network* (WRAN) standard require *channel estimation* (CE) that is both accurate and computationally frugal under mobility. We propose a low-complexity *Modified Pilot-Based Channel Estimation* (MPCE) scheme that operates in the *channel impulse response* (CIR) domain: interpolation weights are computed once per frame and reused across OFDM symbols, eliminating redundant per-symbol estimation while preserving fidelity. Complementing this, we cast pilot placement as an information-theoretic *D-optimal* design—maximize log det of the *Fisher information matrix* (FIM)—and solve it with a greedy exchange using rank-one (Sherman–Morrison) updates under IEEE 802.22 feasibility (guard/direct-current (DC) tone exclusion and minimum spacing). A FIM/*Cramér–Rao bound* (CRB) analysis links pilot spacing and correlation to *mean-squared error* (MSE), explaining when nonuniform pilots help. Simulations under *wide-sense stationary uncorrelated scattering* (WSSUS) Rayleigh fading show that MPCE reduces runtime by up to **78%** versus conventional pilot interpolation while achieving comparable or lower MSE and post-detection *bit-error rate* (BER) for *quadrature phase-shift keying* (QPSK) and *16-ary quadrature amplitude modulation* (16QAM), with the largest gains in the *signal-to-noise ratio* (SNR) range of 10–20 dB. The D-optimal solver converges to a near-uniform layout in our regime (justifying the standard pattern) and departs from uniformity when pilots are scarce or frequency selectivity increases. MPCE thus offers a scalable, hardware-friendly CE approach for wide-area cognitive OFDM links.

Keywords— Channel estimation, OFDM, IEEE 802.22, pilot optimization, cognitive radio, TV white space, complexity analysis, interpolation reuse, mutual information, spectrum efficiency.

1 Introduction

Intelligent transportation systems (ITS) increasingly demand reliable, wide-area wireless connectivity for safety and cooperative perception. Deployed stacks such as IEEE 802.11p/DSRC for V2X have demonstrated feasibility in vehicular contexts [21], yet operation in congested GHz bands limits coverage and link robustness over rural or sparsely served regions. By contrast, sub-GHz TV white spaces (TVWS) offer favorable propagation and regulatory frameworks that can enable long-range links and wide-area networking.

IEEE 802.22 targets TVWS with an OFDM-based PHY/MAC for wireless regional area networks (WRAN) [23, 31]. The standard's scattered pilots and spectral masks are designed for fixed access, but mobility and time selectivity introduce nontrivial channel-estimation (CE) challenges. Recent works report 802.22-oriented channel measurement and modeling [5], scattered-pilot CE under mobility [2], and practical SDR/evaluation platforms [27, 28]; related studies for TVWS WLAN (IEEE 802.11af) highlight similar CE issues in realistic propagation [6]. Classical pilot-aided OFDM CE—LS/LMMSE with interpolation—has been extensively studied, including the impact of pilot layouts (comb/block/scattered) and interpolation domains (time/frequency/DFT) on accuracy and conditioning

[20,36,37]. However, per-symbol interpolation and dense pilot patterns can be computationally demanding on resource-limited receivers, while suboptimal pilot spacing/layout degrades robustness under Doppler and frequency selectivity [2, 6, 8, 36].

This work. We propose a *Modified Pilot-Based Channel Estimation (MPCE)* scheme tailored to IEEE 802.22. MPCE operates in the *CIR domain* (where channel energy is compact), computes interpolation weights *once per frame*, and *reuses* them across OFDM symbols, thereby reducing redundant computation while preserving estimation fidelity. Complementing this, we formulate *information-theoretic pilot placement* as a D-optimal design problem—maximizing the log-determinant of the Fisher information matrix (FIM)—and solve it via a practical greedy Fedorov-exchange algorithm with rank-one (Sherman–Morrison) updates and IEEE 802.22 feasibility masks (guard/DC removal and minimum spacing). This yields a standard-aware pilot set that is information-efficient without incurring per-symbol overhead.

We evaluate MPCE under a WSSUS Rayleigh model aligned with 802.22 deployments [22] and report both estimation MSE and *post-detection* BER for QPSK/16QAM with explicit equalization/detection. In our regime, the D-optimal solver converges to a near-uniform pilot layout (consistent with the standard) and delivers *near-MMSE* accuracy at substantially lower runtime; when pilots are scarce or frequency selectivity increases, the solver departs from uniformity and provides measurable gains. Beyond asymptotics, we quantify operation-level complexity and show that the one-time pilot-selection cost is amortized across frames, leading to low steady-state per-frame cost.

Relation to high-mobility OTFS. OTFS modulation places symbols in the delay–Doppler (DD) domain and is known for Doppler robustness [38, 39]. Recent OTFS receivers for integrated sensing and communication (ISAC) exploit unified variational-inference formulations for joint DD-domain estimation/detection [40]. While our focus is IEEE 802.22 OFDM CE and pilot design, the same principle of *maximizing Fisher information under feasibility constraints* directly extends to DD-domain resource placement, making OTFS/ISAC a promising direction for future work in high-mobility regimes complementary to 802.22.

Key Contributions.

Under IEEE 802.22 constraints, we introduce a low-complexity CIR-domain estimator with frame-wise weight reuse and an information-theoretic (D-optimal) pilot-selection solver, and validate the design end-to-end; the key contributions are:

- **CIR-domain MPCE with frame-wise reuse.** We propose a Modified Pilot-Based Channel Estimator (MPCE) that operates in the CIR domain (energy-compact, well-conditioned) and computes interpolation weights once per frame, then *reuses* them across OFDM symbols. The CSI→equalization→detection pipeline is explicit (Sec. 4.4), so all BER results are end-to-end.
- **Information-theoretic pilot placement with a practical solver.** Pilot selection is cast as D-optimal design (maximize $\log\det(\mathbf{F})$). We implement a greedy Fedorov exchange with Sherman–Morrison rank-one updates under IEEE 802.22 feasibility (guard/DC exclusion, minimum spacing). The add-only greedy objective is monotone submodular (yielding a $(1-1/e)$ factor), and local exchanges further improve solutions in practice (Sec. 4.1.1, Alg. 2).
- **Theory → insight:** *why* and *when* it helps. An FIM/CRB view links pilot spacing/correlation to MSE and predicts regimes where D-optimal placement yields gains (small pilot budget K, stronger frequency selectivity). We add targeted diagnostics—log-det(FIM) convergence, pilot-index maps, and a K-sensitivity study—that explain the observed behavior and recover near-uniform layouts when they are already (near) optimal (Sec. 5).
- **Efficiency with quantified overhead.** We provide operation-level complexity and measured runtime. Pilot selection is a one-time (infrequent) control-plane task amortized across frames; steady-state per-frame work is essentially equalization+FFTs. In our setup this yields up to **78%** execution-time reduction while retaining near-MMSE accuracy (Sec. 5).
- **IEEE 802.22-aware, end-to-end evaluation.** Under standard constraints and a WSSUS Rayleigh model, MPCE consistently lowers MSE and translates this into lower *post-detection* BER for QPSK/16QAM—most notably at 10–20 dB SNR—while the D-optimal solver explains when uniform pilots are already (near) best and when non-uniform designs improve conditioning and BER (Sec. 5).

The remaining portions of this paper are structured as follows: The related works have been discussed in Section 2. Section 3 is for system description and the general familiarization of IEEE 802.22, such as frame structure, signal modeling, etc. The proposed estimation scheme have been explained in Section 4. In Section 5, all simu-

lation results have been shown, and a performance evaluation has been done. Lastly, Section 6 concludes the paper.

2 Related Work

Foundational pilot-aided OFDM estimators include LS and LMMSE with interpolation across data tones; seminal studies analyze pilot layouts (comb/block/scattered) and interpolation domains (time/frequency/DFT), highlighting accuracy–complexity trade-offs and sensitivity to pilot density/placement [36, 37]. DFT-/LPF-based interpolation can denoise but degrades with suboptimal spacing or stronger dispersion [36]. Recent works adapt these ideas to TV white spaces (TVWS) and WLAN variants (e.g., 802.11af), addressing mobility and practical constraints [2,6,22,23,27,28]. Our work differs by (i) operating explicitly in the CIR domain with frame-wise weight reuse (low per-frame cost), and (ii) coupling pilot placement to an information-theoretic (FIM/D-optimal) criterion integrated with an end-to-end receiver.

Temporal trackers (decision-directed, LMS/RLS/Kalman) can reduce explicit pilots but require reliable initialization and may suffer error propagation under mobility; related practical estimation refinements also appear for IoT/OFDM [8]. Sparse/compressive approaches in CIR or delay–Doppler can lower pilot usage in sparse multipath, but introduce iterative cost and model-sensitivity [3, 16, 18, 24]. By contrast, we pursue *CIR-domain estimation with frame-wise weight reuse*, avoiding per-symbol matrix updates while keeping a transparent pilot-aided pipeline.

Pilot placement via mutual information/Fisher information (A-/D-optimality), convex relaxations, and greedy/submodular strategies has been explored in various forms; classic OFDM studies document the role of pilot arrangement on estimator conditioning [36]. Many prior designs assume idealized feasibility (no guard/DC tones, no minimum spacing) and often do not integrate design with an explicit end-to-end receiver and runtime analysis. We instead cast pilot selection as a *D-optimal* design (maximize $\log\det$ of the FIM) and develop a practical greedy Fedorov exchange with Sherman–Morrison rank-one updates, feasibility masks for guard/DC and minimum spacing (IEEE 802.22-aware), and a submodular-optimization view (Sec. 4.2); we analyze convergence, pilot maps, sensitivity to pilot budget, and amortized runtime in Secs. 5.3.2–5.4.

IEEE 802.22 specifies PHY/MAC for WRAN operation in TVWS with strict spectral masks and scattered pilots [23, 31]. Channel modeling/measurement platforms and reliable scattered-pilot estimation geared to 802.22 mobility have been reported in [2,5,27]; related 802.11af (TVWS WLAN) channel-estimation studies provide further practical insights [6]. Analytical modeling of 802.22 WRAN and TVWS coexistence remains an active area [1, 22, 26]. Our evaluation enforces 802.22 feasibility (guard/DC removal, minimum spacing), uses a WSSUS Rayleigh model tailored to TVWS [22], and reports end-to-end MSE/BER with explicit equalization/detection (Sec. 5.1).

Orthogonal Time Frequency Space (OTFS) modulation maps symbols to the delay–Doppler (DD) domain, offering robustness to high Doppler and rapidly time-varying channels [38,39]. In parallel, integrated sensing and communication (ISAC) for OTFS has advanced, including a *unified variational-inference* (VI) OTFS–MIMO receiver that jointly performs estimation/detection in DD [40]. While our focus is IEEE 802.22 OFDM channel estimation and pilot design, the same information-theoretic principle employed here—*maximize Fisher information under feasibility constraints*—naturally extends to DD-domain resource design for OTFS/ISAC; we view this as a promising direction (Sec. 6).

3 SYSTEM DESCRIPTION

3.1 Deployment Scenario: IEEE 802.22 for Rural Area Connectivity

In the proposed deployment scenario Fig 1, a central IEEE 802.22 base station serves as the backbone of the rural connectivity network. This base station is strategically positioned in a location that offers optimal coverage across the target rural area. The IEEE 802.22 base station employs cognitive radio technology to dynamically sense and identify available TV white space channels. This adaptive approach ensures efficient spectrum utilization and minimizes interference with existing TV broadcasts. The base station establishes a reliable and high-speed wireless link with customer premises equipment (CPE), enabling residents and businesses in rural areas to access the internet. To complement the IEEE 802.22 deployment, the scenario also includes the integration of small 5G base stations within the network. These small cells are strategically positioned in areas where additional coverage and capacity are needed, such as densely populated spots or areas with higher data demand. The combination of IEEE 802.22 and 5G technologies creates a hybrid network that offers a seamless and robust connectivity experience. The small 5G base stations provide enhanced data rates, low latency, and support for a wide range of emerging applications, including IoT devices and real-time communication services. This hybrid approach leverages the strengths of

both technologies to ensure comprehensive coverage and optimal performance throughout the rural area. A few vehicles are equipped with communication devices that enable them to act as mobile nodes within the network. These vehicles can serve multiple purposes such as Mobile Coverage Augmentation, Data Collection and Analysis, Emergency Response, and Connectivity.

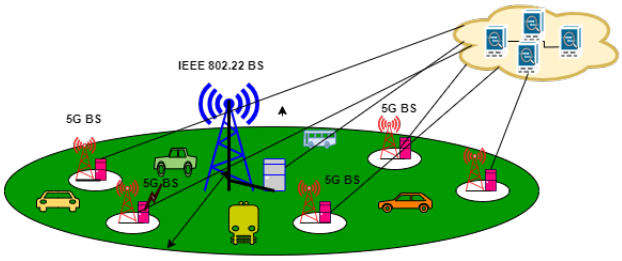

Figure 1: Deployment Scenario

Table 1: The System Parameters of IEEE 802.22 [23]

Parameter	Value
Frequency range	54-862 MHZ
Channel Bandwidth	6,7,8 MHz
Data rate	4.54-22.69 Mbits/s
Transmit EIRP	4 W maximum
Multiple Access Technique	OFDMA
Duplex	TDD
FFT size	2048
CP length	1/4,1/8,1/16,1/32
TV Channel Bandwidth(MHz)	6,7,8
Total Number of subcarriers N_{FFT}	2048
Number of guard subcarriers $N_G(L, DC, R)$	368(184,1,183)
Number of used subcarriers $N_T = N_D + N_P$	1680
Number of Data subcarriers N_D	1440
Number of pilot subcarriers N_P	240
Signal Bandwidth(MHz)	5.63,6.57,7.45

3.2 Channel Statistical Characterization

For performance evaluation, the wireless channel is modeled as a wide-sense stationary uncorrelated scattering (WSSUS) channel with Rayleigh fading statistics. The channel impulse response can be expressed as

$$h(t,\tau) = \sum_{l=0}^{L-1} \alpha_l(t)\,\delta(\tau - \tau_l), \tag{1}$$

where $\alpha_l(t)$ denotes the complex Gaussian fading coefficient of the lth multipath component with variance σ_l^2, and τ_l is the corresponding path delay.

Each $\alpha_l(t)$ is modeled as a zero-mean circularly symmetric complex Gaussian random variable, i.e.,

$$\alpha_l(t) \sim \mathcal{CN}(0, \sigma_l^2), \tag{2}$$

leading to Rayleigh-distributed envelope amplitudes. The power delay profile (PDP) is assumed exponential, i.e., $\sigma_l^2 = \sigma_0^2 e^{-\tau_l/\tau_{\text{rms}}}$, where τ_{rms} is the root-mean-square delay spread.

The temporal correlation of each path is governed by the Jakes Doppler spectrum:

$$R_{\alpha_l}(\Delta t) = \sigma_l^2 J_0(2\pi f_d \Delta t), \tag{3}$$

where f_d is the maximum Doppler frequency and $J_0(\cdot)$ is the zeroth-order Bessel function of the first kind. For our simulations, the maximum Doppler is set to $f_d = 35$ Hz, corresponding to a vehicle speed of $v = 80$ km/h at a carrier frequency of 473 MHz.

The frequency-domain channel response is obtained as the Fourier transform of the impulse response:

$$H(n) = \sum_{l=0}^{L-1} \alpha_l\, e^{-j2\pi n \tau_l/T}, \tag{4}$$

which is used in the channel estimation procedures described in Section 4. This statistical characterization ensures that the Monte Carlo simulations capture both large-scale (path-loss, delay spread) and small-scale (Rayleigh fading, Doppler) phenomena in IEEE 802.22 systems.

3.3 Modulation Formats

In our simulations, we consider Quadrature Phase Shift Keying (QPSK) and 16-Quadrature Amplitude Modulation (16QAM), which are also supported in IEEE 802.22 PHY specifications.

QPSK maps two input bits to one of four constellation points placed equidistantly on the unit circle, with Gray coding employed to minimize bit error probability. The transmitted symbol set is

$$\mathcal{S}_{\text{QPSK}} = \left\{ \pm\frac{1}{\sqrt{2}} \pm j\frac{1}{\sqrt{2}} \right\}. \tag{5}$$

16QAM conveys four input bits per symbol, where each symbol corresponds to one of 16 constellation points arranged in a square grid. Normalized Gray-coded mapping is used to reduce the average symbol energy and

simplify detection:

$$\mathcal{S}_{16\text{QAM}} = \left\{ \pm\frac{1}{\sqrt{10}}(1+2a) \pm j\frac{1}{\sqrt{10}}(1+2b) \,\middle|\, a,b \in \{0,1\} \right\}. \tag{6}$$

The rationale for choosing these two modulation formats is as follows:

- QPSK provides robustness against noise and fading, making it a baseline modulation for performance comparison.
- 16QAM offers higher spectral efficiency but is more sensitive to channel estimation errors, thereby highlighting the benefit of accurate channel estimation methods such as the proposed MPCE.

By including both low-order (QPSK) and higher-order (16QAM) modulations, we demonstrate that the proposed channel estimation technique is effective across different robustness–efficiency trade-offs.

3.4 Brief Review of IEEE 802.22

IEEE 802.22, formulated for Wireless Regional Area Networks (WRANs) functioning in TV white spaces, employs a superframe architecture that facilitates cooperative transmission with expanded cell range. Each 160ms superframe consists of sixteen 10ms frames, partitioned into two unequal subframes featuring a Subchannelization Control Window (SCW). The initial frame comprises a superframe preamble, frame preamble, Superframe Control Header (SCH), and Frame Control Header (FCH), whereas the subsequent frames consist solely of the frame preamble, FCH, and data payload. Coarse frequency synchronization and signal detection are executed via the superframe preamble, which comprises four iterations of the Short Training Sequence (STS) and the cyclic prefix (CP). Precise synchronization and channel estimation utilize the frame preamble, which consists of two repetitions of the Long Training Sequence (LTS) and the Cyclic Prefix (CP). Each frame encompasses 60 subchannels within the frequency domain.

Pilot symbols are included in seven OFDM symbols and seven subcarriers according to a predetermined pattern for both uplink and downlink transmissions. Pilots are positioned prior to interleaving in the uplink and subsequently reordered at the base station. The system presumes a rural implementation with a maximum delay spread of 21 and coverage extending to 30km, leading to frequency-selective fading and Doppler phenomena. IEEE 802.22 accommodates 12 modulation and coding combinations—QPSK, 16QAM, and 64QAM across four coding rates—and delineates 14 transmission modes, with Mode 1 designated for control signals. The 8.1MHz bandwidth consists of 2048 orthogonal subcarriers organized into 60 subchannels, each containing 28 carriers, of which 24 are designated for data and 4 for pilot symbols. Furthermore, 368 subcarriers are designated as guard/null tones to mitigate inter-carrier interference. Pilot-assisted channel assessment is crucial for mitigating time-frequency distortions and guaranteeing dependable communication in dynamic multipath settings. environments.

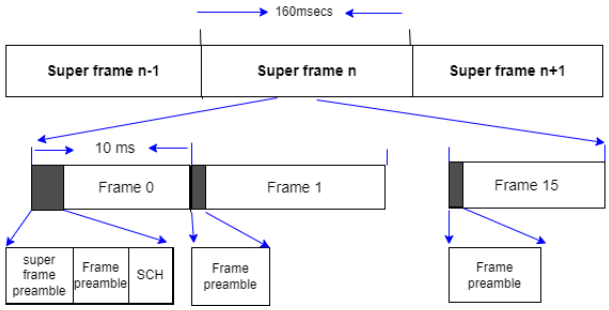

Figure 2: Frame structure of IEEE 802.22 System [23]

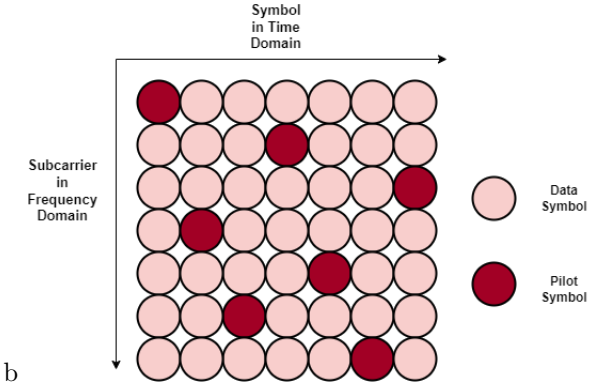

Figure 3: Standard Pilot Pattern of IEEE 802.22 [23]

Pilot symbols—known reference signals inserted at predefined intervals—enable receivers to estimate the channel response by observing distortions during transmission. This estimation mitigates channel impairments such as fading and distortion, enhancing detection accuracy.

In highly mobile, long-delay multipath channels, frequency-selective fading and Doppler shifts reduce channel coherence. The coherence time and bandwidth with 50% correlation are given as:

$$T_{c,50\%} = \frac{0.423}{f_{d,\max}}, \quad BW_{c,50\%} = \frac{1}{5T_{\text{rms}}} \tag{7}$$

where $f_{d,\max}$ and T_{rms} are the maximum Doppler frequency and RMS delay spread, respectively.

In IEEE 802.22, channel estimation over 14 OFDM symbols is performed using linear interpolation in the fre-

quency domain. Let $h_{m,m}$ denote the pilot symbol channel value in the m^{th} symbol and n^{th} subcarrier. The estimated channel between pilot positions in the frame preamble is:

$$h_{0,n} = |h_{0,n}| \cos\theta_{0,n} + j|h_{0,n}| \sin\theta_{0,n} \tag{8}$$

where $\theta_{0,n}$ represents the phase rotation between pilot symbols.

Zero Padding (ZP) further enhances OFDM robustness. In multiband OFDM (MB-OFDM), the guard interval may be set to zero. However, symbol timing offsets (STO) may introduce FFT discontinuities. To preserve orthogonality, a portion of the next symbol's guard interval is copied and prepended to the current symbol, mitigating inter-channel interference.

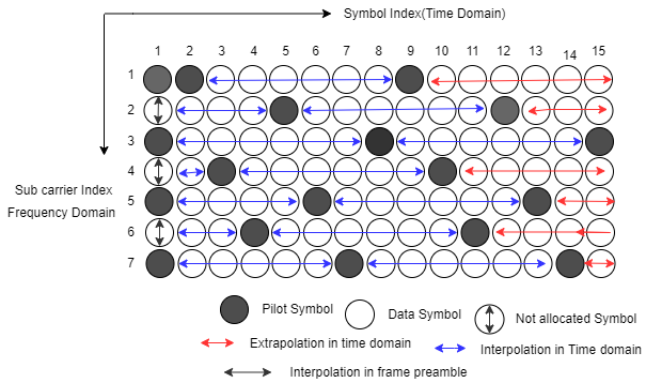

Figure 4: Downstream Sub Frame

4 Proposed Method

In this section, we present the Modified Pilot-Based Channel Estimation (MPCE) method that has the goal of optimizing the trade-off between computational complexity and estimation accuracy. In contrast to traditional techniques, MPCE carefully chooses pilot subcarriers to increase estimation effectiveness without sacrificing the precision of channel interpolation. The Modified Pilot Method presents a hybrid subcarrier grouping technique that makes use of both neighboring and non-adjacent subcarriers, in contrast to the Pilot Method, which solely depends on adjacent subcarriers for estimation. This method improves the reliability of interpolation while minimizing unnecessary computations, hence increasing efficiency without compromising precision. Consider an OFDM-based communication system with N total subcarriers. The received signal at subcarrier n is given by:

$$Y(n) = H(n)X(n) + W(n), \tag{9}$$

where,$Y(n)$ represents the received signal, $X(n)$ is the transmitted symbol, $H(n)$ is the channel frequency response at subcarrier n, $W(n) \sim \mathcal{CN}(0, \sigma^2)$ is the additive white Gaussian noise (AWGN).

The objective of channel estimation is to approximate $H(n)$ using only a subset of pilot subcarriers$\{P_k\}$, where $k = 1, 2, \ldots, K$ and $K \ll N$.

Pilot Selection Strategy: In general the conventional methods select evenly spaced pilots or densely adjacent pilots. However, these selection leads to high interpolation error or additional computations. Our proposed method optimizes pilot selection employing a hybrid strategy:

$$P_k^* = \{p_1, p_3, p_6, p_{10}, p_{15}, \ldots\}, \tag{10}$$

where, P_k^* includes both adjacent and non-adjacent subcarriers, guaranteeing (1) expanded channel coverage by the use of subcarriers that provide varied channel information (2) diminished computational duplication by reducing interpolation overlap (3) Optimal selection employing an information-theoretic methodology.

Theorem 4.1 (Existence and Uniqueness)**.** *Let P_k be the selected pilot subcarriers and let $H(P_k)$ be the corresponding known channel values. There exists a unique interpolation function $f(n)$ such that:*

$$f(P_k) = H(P_k), \quad \forall k = 1, 2, \ldots, K \tag{11}$$

and for all subcarriers n (non-pilot positions),

$$H(n) \approx f(n). \tag{12}$$

Proof. Define the Lagrange interpolating polynomial as:

$$\hat{H}(n) = \sum_{k=1}^{K} H(P_k) L_k(n), \tag{13}$$

where $L_k(n)$ are the Lagrange basis polynomials, given by:

$$L_k(n) = \prod_{\substack{j=1 \\ j \neq k}}^{K} \frac{n - P_j}{P_k - P_j}. \tag{14}$$

This function satisfies the uniqueness property because:

1. The polynomial of degree $K - 1$ is uniquely determined by K data points.

2. The Modified Pilot Method ensures that the selection of P_k is non-redundant, guaranteeing that the denominator does not vanish, thereby ensuring a unique solution.

Thus, the interpolation function is well-posed and uniquely determined. □

Subcarrier Grouping Strategy: The principal advancement in the Modified Pilot Method is the enhanced selection of pilot subcarriers. The approach selectively selects subcarriers that provide substantial channel information, rather than depending exclusively on neighboring pilots, while minimizing excessive interpolation steps. The subcarrier grouping process follows these principles:

(a)Expanded Subcarrier Relationships: Rather than utilizing solely consecutive subcarriers, chosen pilots encompass pairs that extend across several subcarrier indices. This facilitates a more comprehensive display of channels. (b) Selective Redundancy Reduction: Overlapping pilot subcarriers from the conventional Pilot Method are eliminated, hence avoiding superfluous computations while maintaining essential channel attributes. (c)Hybrid Pilot Selection: This approach incorporates both neighboring and non-adjacent pilot subcarriers, hence improving interpolation performance while maintaining computing efficiency to estimate. Mathematically, if $H(n)$ represents the actual channel response for subcarrier n, and P_k denotes the set of selected pilot subcarriers, the estimation process can be expressed as:

$$\hat{H}(n) = f(P_k) + \varepsilon \tag{15}$$

where $f(P_k)$ represents the interpolation function applied to selected pilot subcarriers and ε is the estimation error.

For each pilot subcarrier P_k, we define an optimized grouping function:

$$S_k = \left\{ \frac{\mathrm{rx}(i,j)}{\mathrm{tx}(i,j)} \mid i,j \in P_k \right\} \tag{16}$$

where, $\mathrm{rx}(i,j)$ and $\mathrm{tx}(i,j)$ represent the received and transmitted signals for a given subcarrier pair. This adaptive grouping offers better frequency diversity.

The estimated channel response $\hat{H}(n)$ is computed using a combination of Fast Fourier Transform (FFT) interpolation and linear extrapolation.

For pilot subcarriers P_k^*, FFT-based interpolation reconstructs the missing channel values as:

$$\hat{H}(n) = \sum_{k=1}^{K} w_k H(P_k), \tag{17}$$

where the interpolation weights w_k are obtained using least squares estimation:

$$\mathbf{w} = (\mathbf{P}^H \mathbf{P})^{-1} \mathbf{P}^H \mathbf{H}. \tag{18}$$

For subcarriers outside the pilot range, linear extrapolation is applied,

$$\hat{H}(n) = an + b, \tag{19}$$

where coefficients (a, b) are estimated using least squares regression over the last two pilot subcarriers. The estimation accuracy is measured using the Mean Square Error (MSE):

$$MSE = \frac{1}{M} \sum_{n=1}^{M} |H(n) - \hat{H}(n)|^2. \tag{20}$$

Theorem 4.2 (MSE Upper Bound)**.** *Let $H(n)$ be the actual channel response, and let $\hat{H}(n)$ be the estimated response using the Modified Pilot Method. The interpolation error is bounded as follows:*

$$MSE_{modified} = \mathbb{E}\left[|H(n) - \hat{H}(n)|^2\right] \leq \frac{C}{K} \sum_{k=1}^{K} |P_k^* - H(n)|, \tag{21}$$

where C is a constant that depends on the interpolation function and the smoothness of the channel.

Proof. Using the Taylor series expansion, the interpolation error at a non-pilot subcarrier n is given by:

$$H(n) - \hat{H}(n) = \frac{H^{(r)}(\xi)}{r!} \prod_{k=1}^{K} (n - P_k), \tag{22}$$

where ξ is some intermediate point in the interpolation interval, and r is the order of the interpolating polynomial.

Applying Jensen's inequality, we take the expectation on both sides:

$$\mathbb{E}\left[|H(n) - \hat{H}(n)|^2\right] \leq \frac{C}{K} \sum_{k=1}^{K} |P_k^* - H(n)|. \tag{23}$$

Since the Modified Pilot Method strategically places pilots to minimize interpolation gaps, this bound is tighter than the one obtained in the conventional Pilot Method.

Thus, the MSE of the Modified Pilot Method is lower than conventional pilot-based estimations. □

4.1 Information-Theoretic Pilot Selection

The Modified Pilot Method's key benefit is its capacity to optimize pilot selection by optimizing the information content of the received signals. We formalize this by employing an information-theoretic framework.

Definition 1 (Mutual Information for Pilot Selection)**.** *The optimal set of pilot subcarriers P_k^* maximizes the mutual information between the received signal Y and the channel response H, conditioned on the selected pilot subcarriers:*

$$I(Y; H \mid P_k) = H(Y) - H(Y \mid H, P_k), \tag{24}$$

where, $H(Y)$ represents the entropy of the received signal. $H(Y \mid H, P_k)$ represents the remaining uncertainty after observing pilots.

Theorem 4.3 (Optimal Pilot Set Maximization)**.** *The optimal pilot set P_k^* satisfies the mutual information maximization criterion:*

$$P_k^* = \arg\max_{P_k} I(Y; H \mid P_k). \tag{25}$$

Proof. The pilot subcarriers are selected to maximize the Fisher Information Matrix (FIM), which quantifies the amount of information contained in the observed pilots. The FIM is given by:

$$J(P_k) = \sum_{k=1}^{K} \frac{1}{\sigma_k^2} \nabla H(P_k) \nabla H(P_k)^T. \tag{26}$$

The determinant $J(P_k)$ represents the total information captured by the selected pilot subcarriers. To ensure maximum information gain, the Modified Pilot Method selects pilots to maximize:

$$P_k^* = \arg\max_{P_k} \det J(P_k). \tag{27}$$

Since maximizing $\det J(P_k)$ corresponds to minimizing estimation uncertainty, the pilot set P_k^* obtained via this criterion is information-theoretically optimal.

Thus, the Modified Pilot Method achieves superior channel estimation by selecting the most informative subcarriers, ensuring a balance between accuracy and computational efficiency. □

4.2 Solving the Pilot-Selection Criterion and Practical Insights

Equation (27) casts pilot placement as an information–theoretic design problem. We model the pilot observation on subcarrier set $\mathcal{P} \subset \{0, \dots, N-1\}$ by the linear Gaussian model

$$\mathbf{y}_{\mathcal{P}} = \mathbf{X}_{\mathcal{P}} \mathbf{h} + \mathbf{w}, \qquad \mathbf{w} \sim \mathcal{CN}(\mathbf{0}, \sigma^2 \mathbf{I}), \tag{28}$$

where $\mathbf{h} \in \mathbb{C}^L$ are the L-tap CIR coefficients and $\mathbf{X}_{\mathcal{P}} \in \mathbb{C}^{N_p \times L}$ is the pilot design matrix whose p-th row is $\mathbf{x}_p^{\mathrm{H}} = \big[1,\ e^{-j\frac{2\pi}{N}p},\ \dots,\ e^{-j\frac{2\pi}{N}p(L-1)}\big]$ for $p \in \mathcal{P}$. The (expected) Fisher information matrix (FIM) for $\mathbf{h}$ is

$$\mathbf{F}(\mathcal{P}) = \frac{1}{\sigma^2} \mathbf{X}_{\mathcal{P}}^{\mathrm{H}} \mathbf{X}_{\mathcal{P}} = \sum_{p \in \mathcal{P}} \underbrace{\frac{1}{\sigma^2} \mathbf{x}_p \mathbf{x}_p^{\mathrm{H}}}_{\triangleq\, \mathbf{u}_p \mathbf{u}_p^{\mathrm{H}}}, \tag{29}$$

so by the complex Cramér–Rao bound $\mathrm{cov}(\hat{\mathbf{h}}) \succeq \mathbf{F}(\mathcal{P})^{-1}$ for any unbiased estimator. Maximizing $\det \mathbf{F}$ minimizes the generalized variance $\det(\mathrm{cov}(\hat{\mathbf{h}}))$, yielding the classical *D-optimal* criterion

$$\mathcal{P}^\star = \arg \max_{\mathcal{P} \subset \{0,\dots,N-1\},\, |\mathcal{P}| = N_p} \log\det\big(\mathbf{F}(\mathcal{P})\big). \tag{30}$$

Because the CFR satisfies $\mathbf{H} = \mathbf{D}\mathbf{h}$ with $\mathbf{D}$ the $N \times L$ DFT submatrix, the frequency-domain MSE obeys $\mathbb{E}\|\mathbf{H} - \hat{\mathbf{H}}\|_2^2 = \mathrm{tr}\big(\mathbf{D}\,\mathrm{cov}(\hat{\mathbf{h}})\,\mathbf{D}^{\mathrm{H}}\big)$, so maximizing $\det \mathbf{F}$ tightens the lower bound for both Channel Impulse Response (CIR) and Channel Frequency Response (CFR) estimates.

Greedy (Fedorov) exchange with rank-one updates. (27) is combinatorial (NP-hard). We use a Fedorov-type exchange: swap $i \in \mathcal{P}$ with $j \in \mathcal{C} \backslash \mathcal{P}$ (with $\mathcal{C}$ masking guard/DC and enforcing spacing $\Delta_{\min}$) if it increases $f(\mathcal{P}) = \log\det \mathbf{F}$. Using the matrix-determinant lemma and Sherman–Morrison, marginal gains are computed without re-inverting $\mathbf{F}$:

$$\Delta_{\mathrm{add}}(q) = \log\big(1 + \mathbf{u}_q^H \mathbf{F}^{-1} \mathbf{u}_q\big), \tag{31}$$

$$\Delta_{\mathrm{swap}} = \log(1-\beta) + \log(1+\alpha'), \tag{32}$$

$$\beta = \mathbf{u}_i^H \mathbf{F}^{-1} \mathbf{u}_i, \quad \alpha' = \mathbf{u}_j^H \mathbf{F}_{-i}^{-1} \mathbf{u}_j, \tag{33}$$

$$\mathbf{F}_{-i}^{-1} = \mathbf{F}^{-1} + \frac{1}{1-\beta} \mathbf{F}^{-1} \mathbf{u}_i \mathbf{u}_i^H \mathbf{F}^{-1},\ \mathbf{F}_{-i} = \mathbf{F} - \mathbf{u}_i \mathbf{u}_i^H. \tag{34}$$

We regularize $\mathbf{F} \leftarrow \mathbf{F} + \varepsilon \mathbf{I}$ (e.g., $\varepsilon = 10^{-6}$) for numerical stability when the initial set is ill-conditioned. The set function $f(\mathcal{P}) = \log\det\big(\varepsilon \mathbf{I} + \sum_{p \in \mathcal{P}} \mathbf{u}_p \mathbf{u}_p^H\big)$ is monotone submodular under $|\mathcal{P}| = N_p$; hence an add-only greedy achieves a $(1 - 1/e)$ factor, while exchanges (2-opt/Fedorov) further refine the solution empirically.

Complexity. Each rank-one update/downdate costs $\mathcal{O}(L^2)$; one outer sweep that tests all (i, j) pairs is $\mathcal{O}\big(L^2\, N_p\, (|\mathcal{C}| - N_p)\big)$. Since $L \ll N$, the dominant cost lies in a few sweeps of low-dimensional (L) updates, and—per Sec. 5.4—the selection is run infrequently and amortized across many frames.

Algorithm 1 Greedy D-Optimal Pilot Selection (Fedorov Exchange with Rank-One Updates:)

Require: N (subcarriers), N_p (pilot budget), $\mathcal{C}$ (candidates without guard/DC), $\Delta_{\min}$, noise variance σ^2
Ensure: $\mathcal{P}$ maximizing $\log\det(\mathbf{F}(\mathcal{P}))$

$\mathcal{P} \leftarrow \text{UniformSpacing}(\mathcal{C}, N_p)$; $\mathbf{F} \leftarrow \sum_{p\in\mathcal{P}} \mathbf{u}_p\mathbf{u}_p^{\mathrm{H}} + \varepsilon\mathbf{I}$; $\mathbf{G} \leftarrow \mathbf{F}^{-1}$; $L \leftarrow \log\det\mathbf{F}$
repeat
  improved $\leftarrow$ **false**
  for each $i \in \mathcal{P}$ **do**
    $\beta \leftarrow \mathbf{u}_i^{\mathrm{H}}\mathbf{G}\mathbf{u}_i$; **if** $\beta \geq 1-\delta$ **then continue** ▷ $\delta > 0$ safety
    $\mathbf{G}_{-i} \leftarrow \mathbf{G} + \dfrac{\mathbf{G}\mathbf{u}_i\mathbf{u}_i^{\mathrm{H}}\mathbf{G}}{1-\beta}$ ▷ downdate for removal
    for each $j \in \mathcal{C} \setminus \mathcal{P}$ **do**
      if $\text{SpacingViolation}\big((\mathcal{P}\setminus\{i\})\cup\{j\}, \Delta_{\min}\big)$ **then continue**
      $\alpha' \leftarrow \mathbf{u}_j^{\mathrm{H}}\mathbf{G}_{-i}\mathbf{u}_j$; $\Delta \leftarrow \log(1-\beta) + \log(1+\alpha')$
      if $\Delta > 0$ **then**
        $\mathbf{G} \leftarrow \mathbf{G}_{-i} - \dfrac{\mathbf{G}_{-i}\mathbf{u}_j\mathbf{u}_j^{\mathrm{H}}\mathbf{G}_{-i}}{1+\alpha'}$ ▷ rank-one add
        $\mathcal{P} \leftarrow (\mathcal{P}\setminus\{i\})\cup\{j\}$; $L \leftarrow L + \Delta$; *improved* $\leftarrow$ **true**; **break**
      end if
    end for
    if *improved* **then break**
    end if
  end for
until *improved* = **false or** maxIters reached
return $\mathcal{P}$

Intuition. Each pilot contributes the rank-one matrix $\mathbf{u}_p\mathbf{u}_p^{\mathrm{H}}$ to $\mathbf{F}$. The greedy rule accepts the swap with the largest marginal increase in $\log\det\mathbf{F}$; early iterations remove near-collinear (redundant) rows of $\mathbf{X}_\mathcal{P}$ and insert more "orthogonal" ones, rapidly improving conditioning (large positive Δ). Once $\mathbf{F}$ is well-conditioned, marginal gains shrink and the curve plateaus. For WSSUS Rayleigh channels with moderate N_p, the correlation is Toeplitz-like and uniform spacing already spreads $\{\mathbf{x}_p\}$ nearly orthogonally in the L-dimensional subspace—hence the solver often converges to (or very near) the IEEE 802.22 uniform pattern. In more frequency-selective channels, tighter pilot budgets, or nonuniform candidate masks, the same solver yields non-uniform designs with strictly larger $\log\det\mathbf{F}$ and lower CRB.

4.3 Analytical Characterization of Channel Estimation Error with Varying Pilot Spacing

To analytically support the observed superiority of the Modified Pilot-Based Channel Estimation (MPCE) method, we derive the interpolation error as a function of pilot spacing and channel frequency correlation. This allows us to quantify the impact of pilot placement strategies on mean squared error (MSE) performance.

We assume the frequency-selective Rayleigh fading channel $H(n)$ is wide-sense stationary with autocorrelation function:

$$R_H(\Delta) = \mathbb{E}[H(n)H^*(n+\Delta)] = \sigma_h^2 \cdot \operatorname{sinc}\left(\frac{\Delta}{\Delta_f}\right), \quad (35)$$

where Δ_f is the coherence bandwidth, and Δ is the subcarrier spacing between the point of estimation and the nearest pilot. This model captures the correlation decay across frequency in multipath channels.

Following MMSE interpolation theory, the variance of the estimation error when interpolating between two pilot subcarriers spaced by Δ is given by:

$$\sigma_{\text{int}}^2(\Delta) = R_H(0) - \frac{R_H(\Delta)^2}{R_H(0)}. \quad (36)$$

This expression shows that the interpolation error decreases with increasing correlation between pilot and estimated subcarrier — i.e., with smaller Δ or larger Δ_f.

Let $P_k \subset \{1, \ldots, N\}$ denote the set of pilot subcarrier indices, and let Δ_n be the distance from subcarrier $n \notin P_k$ to its nearest pilot. Then, the overall MSE due to interpolation is approximately:

$$\begin{aligned}\text{MSE}_{\text{total}} &\approx \frac{1}{N-K}\sum_{n\notin P_k}\sigma_{\text{int}}^2(\Delta_n)\\ &= \frac{1}{N-K}\sum_{n\notin P_k}\left(\sigma_h^2 - \frac{R_H(\Delta_n)^2}{\sigma_h^2}\right) \quad (37)\end{aligned}$$

The differences in MSE among the three methods can now be understood based on their respective pilot configurations:

- **Normal Method:** Sparse, evenly spaced pilots result in large Δ_n, reducing $R_H(\Delta_n)$ and increasing MSE.
- **Pilot Method:** Densely packed pilots reduce Δ_n, minimizing MSE but at high computational cost due to per-symbol interpolation.

- **Modified Pilot Method (MPCE):** Strategically selected adjacent and non-adjacent pilots optimize the trade-off, keeping Δ_n moderate and minimizing redundant overlap. This yields low MSE at significantly reduced complexity.

Table 2: Simulation Parameters

Parameter	Value
Center Frequency	473MHZ
Channel Bandwidth	6MHz
Sampling Frequency	6.856 MHz
Symbol Rate	2678symbols/s
Maximum CFO	1892Hz
Channel Model	AWGN and Rayleigh
Velocity	80kmph
Maximum Doppler Frequency	35Hz

4.4 Procedure of the Modified Pilot Method: Algorithm and IEEE 802.22 Demonstration

With a 90% percent correlation, the coherence bandwidth (BW_c) is expressed as $BW_{c,90\%} = \frac{1}{50T_{rms}}$ [24]. The frequency of $BW_{c,90\%}$ is 7.2 kHz, which is nearly double the space between sub-carriers. This indicates that neighboring sub-carrier channel fluctuations are essentially coherent and the interpolation interval can be expanded by efficiently exploiting adjacent sub-carrier pilot symbols. The channel estimation process is described below.

Let N be the total number of subcarriers and $\mathcal{P} = \{P_1, P_2, \ldots, P_K\}$ denote the candidate pilot configurations across K clusters. The channel response at pilot positions P_k is denoted as $H(P_k)$, corrupted by additive noise with variance σ_k^2.

1) Informative Pilot Selection via Mutual Information

Unlike fixed pilot patterns, MPCE dynamically evaluates the informativeness of each pilot configuration using mutual information between the received signal Y and the channel realization H:

$$I_k = H(Y) - H(Y \mid H, P_k), \tag{38}$$

where $H(\cdot)$ denotes differential entropy. The pilot set maximizing this information is selected:

$$P_k^* = \arg\max_{P_k \in \mathcal{P}} I_k. \tag{39}$$

This ensures that the chosen pilots contribute maximally to channel observability under bandwidth and energy constraints.

2) Pilot Refinement via Fisher Information Maximization

To further improve estimation precision, we introduce a refinement step that leverages the Fisher Information Matrix (FIM) associated with the chosen pilot set:

$$\mathbf{J} = \sum_{k=1}^{K} \frac{1}{\sigma_k^2} \nabla H(P_k^*) \nabla H(P_k^*)^\top, \tag{40}$$

where $\nabla H(P_k^*)$ denotes the gradient of the channel response. The pilot positions are adjusted to maximize the determinant of $\mathbf{J}$, yielding the most statistically efficient configuration:

$$\max_{P_k^*} \det(\mathbf{J}). \tag{41}$$

3) MMSE-Based Weighted Interpolation

Let $\mathbf{P}$ be the design matrix constructed from P_k^*. The interpolation weights are derived using the MMSE criterion:

$$\mathbf{w} = (\mathbf{P}^{\mathsf{H}}\mathbf{P})^{-1}\mathbf{P}^{\mathsf{H}} H(P_k^*). \tag{42}$$

The interpolated channel estimates for subcarriers $n \notin P_k^*$ are then computed as:

$$\hat{H}(n) = \sum_{k=1}^{K} w_k H(P_k^*). \tag{43}$$

This approach preserves spatial-spectral channel correlation while ensuring computational tractability.

4) Robust Extrapolation for Unobserved Subcarriers

To handle subcarriers outside the pilot span—typically prone to edge effects—we apply a linear least-squares (LS) regression over P_k^*:

$$(a, b) = \mathrm{LS}(P_k^*, H(P_k^*)), \tag{44}$$

yielding an affine model for extrapolation:

$$\hat{H}(n) = an + b. \tag{45}$$

This model captures underlying spectral trends, mitigating boundary-induced degradation.

5) Quality Metric: Mean Squared Error (MSE)

The final estimation quality is quantified using the normalized MSE:

$$\mathrm{MSE} = \frac{1}{M} \sum_{n=1}^{N} \left| H(n) - \hat{H}(n) \right|^2, \tag{46}$$

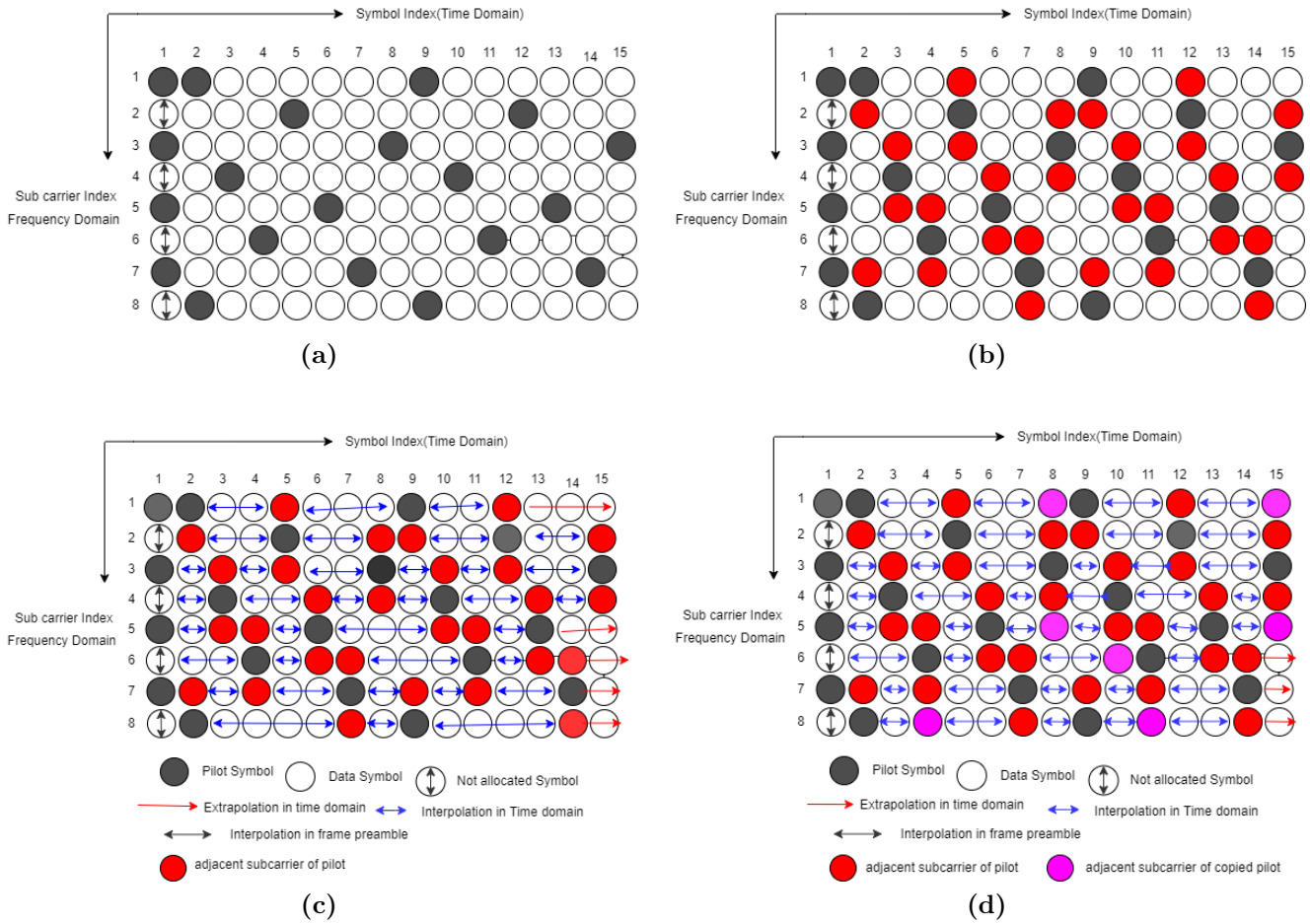

Figure 5: **(a)** Frame preamble interpolation between pilot symbols **(b)** Adjacent sub carriers copying process. **(c)** In the time domain, Extrapolation and Interpolation **(d)** Adjacent sub carriers copying process

where M denotes the number of Monte Carlo realizations or ensemble averaging trials.

The proposed MPCE method synthesizes data-driven pilot allocation with robust statistical estimation, offering a scalable and channel-adaptive solution suitable for high-mobility and large-scale multicarrier networks.

The frame preamble between the pilot symbols is first estimated using zero padding interpolation (Fig. 7(a)). The channel oscillations are then replicated from nearby sub-carrier pilot symbols (Fig. 7(b)). These sample symbols are data symbols with channel fluctuations taken from pilot symbols in surrounding sub-carriers. To reduce the extrapolation range and decrease the interpolation interval as much as feasible, all nearby sub-carriers with pilot symbols are utilized.

In the case of Sub-carrier 4, for instance, the channel variation of the pilot symbol (Symbol 15) from Sub-carrier 3 is replicated to Sub-carrier 4 to reduce the extrapolated range (extrapolated length is entirely removed in this scenario), and then the channel variation of the pilot symbol (Symbol 12) from Sub-carrier 5 is transferred to Sub-carrier 4 to reduce the interpolation period between the Pilot symbol (Symbol 9) and the sample symbol (Symbol 12 and Symbol 14).

To begin, zero padding interpolation is used to estimate the channel fluctuations in the frame preamble between pilot symbols (Fig. 5(c)). The channel fluctuations are then duplicated from adjacent sub-carrier pilot symbols (Fig. 5(d)). In the following, data symbols channel taken from the pilot symbols in neighboring sub-carriers are referred to as sample symbols.

All adjacent sub-carrier variations with pilot symbols are used to limit the extrapolation range and shorten the interpolation interval as much as possible. In the case of Sub-carrier 4, for example, Sub-carrier 3's chan-

nel variant of a pilot symbol in Symbol 15 is transferred to Sub-carriers 4 and 5 to decrease the extrapolated interval (extrapolated size is completely removed in this case), and the pilot symbol's channel variation (Symbol 8) from Sub-carrier 3 is subsequently transferred to Sub-carrier 1 to decrease the interpolation period between sample symbol (Symbol 6) and the pilot symbol (Symbol 5) (Symbol 8).

Algorithm 2 Greedy D-Optimal Pilot Selection (Fedorov Exchange)

Require: N (total subcarriers), N_p (number of pilots), $\mathcal{C}$ (candidate set)
Ensure: Pilot set $\mathcal{P}$ maximizing $\log\det(J)$
Initialize $\mathcal{P} \leftarrow N_p$ uniformly spaced pilots
Compute Fisher matrix $J \leftarrow \sum_{p\in\mathcal{P}} u_p u_p^\top$
$L \leftarrow \log\det(J)$
repeat
  improved $\leftarrow$ **false**
  for each $i \in \mathcal{P}$ **do**
    Form reduced matrix J_{-i} by removing i using Sherman–Morrison
    for each $j \in \mathcal{C} \setminus \mathcal{P}$ **do**
      Compute $J' = J_{-i} + u_j u_j^\top$
      $\Delta \leftarrow \log\det(J') - L$
      if $\Delta > 0$ **then**
        $\mathcal{P} \leftarrow (\mathcal{P} \setminus \{i\}) \cup \{j\}$
        $J \leftarrow J', \quad L \leftarrow L + \Delta$
        improved $\leftarrow$ **true**
        break
      end if
    end for
    if improved **then**
      break
    end if
  end for
until improved = **false**
return $\mathcal{P}$

4.5 Recursive Weight Update and CSI Generation

An important aspect of the proposed Modified Pilot-Based Channel Estimation (MPCE) is its recursive weight update mechanism and the subsequent use of estimated coefficients for channel state information (CSI) generation. This subsection elaborates these two steps for clarity.

4.5.1 Recursive Weight Update

In the MPCE scheme, interpolation weights are computed using the MMSE criterion based on the selected pilot subcarriers P_k^*. As described in (12), the interpolation weights are given by

$$\mathbf{w} = (P^H P)^{-1} P^H H(P_k^*), \tag{47}$$

where P is the pilot design matrix and $H(P_k^*)$ represents the channel frequency response at the pilot subcarriers.

Unlike conventional pilot-aided methods, these weights are computed only once per OFDM frame. For each subsequent OFDM symbol in the frame, the same set of weights is recursively reapplied, thereby eliminating redundant computations. In channels with mobility, the pilot set is periodically updated using the information-theoretic selection criterion in (27). This ensures that the interpolation weights $\mathbf{w}$ adapt to the most informative subcarriers at the beginning of each frame, while symbol-level reuse preserves computational efficiency.

4.5.2 CSI Generation

The interpolated channel coefficients $\hat{H}(n)$ obtained from (11)–(13) are directly used to construct the CSI matrix required for equalization and detection. Specifically, for a received OFDM symbol $Y(n)$, equalization is performed as

$$\hat{X}(n) = \frac{Y(n)}{\hat{H}(n)}, \quad n = 1, 2, \ldots, N, \tag{48}$$

where $\hat{X}(n)$ is the equalized symbol estimate.

The equalized symbols are subsequently passed through a minimum-distance detector for the chosen modulation format (QPSK or 16QAM). For example, the detected symbol $\hat{s}$ is obtained as

$$\hat{s} = \arg\min_{s\in\mathcal{S}} \left| \hat{X}(n) - s \right|^2, \tag{49}$$

where $\mathcal{S}$ denotes the modulation constellation set.

This process ensures that CSI derived from $\hat{H}(n)$ is explicitly exploited in symbol equalization and detection. By integrating one-time interpolation, recursive weight reuse, and explicit CSI construction, the MPCE scheme achieves a favorable trade-off between computational efficiency and estimation accuracy.

4.6 Complexity Analysis

In modern wireless communication systems, Orthogonal Frequency Division Multiplexing (OFDM) is widely utilized due to its resilience against multipath fading and efficient spectral utilization. However, accurate channel estimation is essential for reliable data transmission, especially in high-mobility scenarios. The three widely

used channel estimation techniques—Normal Method, Pilot Method, and Modified Pilot Method—differ significantly in their computational cost and estimation accuracy. A comprehensive complexity analysis is critical to evaluating the trade-offs between computational efficiency, memory usage, and system performance. In this section, we systematically analyze the computational complexity, execution time, and scalability of these estimation techniques.

Asymptotic Complexity Analysis: Channel estimation involves pilot symbol insertion, interpolation, and equalization to recover the transmitted data. The complexity of each method is determined by (a) the number of pilots and subcarriers (b)the type of interpolation used and, (c)the redundancy in computations.

To approximate the missing channel coefficients, the Normal Method employs simple linear interpolation. Given that N is the number of subcarriers, the computational complexity of this approach is $O(N)$. In essence, this approach consists of two operations: equalization and demodulation ($O(N)$) and linear interpolation ($O(N)$). The memory footprint of this approach is minimal. Although computationally efficient, this approach has poor estimation accuracy, which limits its applicability in dynamic wireless situations.

The Pilot Method estimates missing channel coefficients through densely allocated pilot subcarriers and employs spline-based interpolation to recover adjacent channel responses. Due to the frequent pilots placement and redundancy in interpolation operations, the computational complexity of this approach scales quadratically with the number of subcarriers, i.e., $O(N^2)$. The method mainly involves spline interpolation, contributing operations $O(N^2)$, alongside equalization and demodulation steps, each requiring $O(N)$. In addition to the high computational cost, this method incurs a significant memory footprint due to the storage of dense pilot information and intermediate interpolation values. Although the Pilot Method offers high estimation accuracy, its substantial resource demands limit its applicability in real-time systems with large-scale subcarrier configurations.

The Modified Pilot Method introduces an optimized pilot selection strategy to minimize redundant interpolation while preserving high estimation accuracy. By adaptively determining pilot positions based on channel variability, this method reduces unnecessary computations typically present in dense pilot schemes. The overall computational complexity is $O(N \log N)$, striking a balance between efficiency and accuracy. The key operations involved include adaptive pilot selection ($O(N \log N)$), efficient interpolation ($O(N)$), and standard equalization and demodulation ($O(N)$). The memory footprint is moderate, as the method avoids excessive pilot allocation while still storing essential pilot and interpolation data. Owing to its favorable trade-off between performance and complexity, the Modified Pilot Method is particularly well-suited for real-time OFDM systems operating under resource constraints.

To evaluate how computational cost scales with the number of subcarriers N, we also analyze the interpolation overhead per method, the execution time as a function of N, and the theoretical and empirical performance trends.

To substantiate the theoretical complexity of each channel estimation method, we conducted simulations to measure execution time as a function of the number of subcarriers N. The Normal Method exhibited linear complexity, with execution time growing proportionally to $T(N) \approx kN$, where k is a constant. In contrast, the Pilot Method demonstrated quadratic growth, with execution time approximated by $T(N) \approx kN^2$, primarily due to redundancy introduced by dense pilot-based interpolation. The Modified Pilot Method, which employs adaptive pilot placement and efficient interpolation strategies, achieved log-linear complexity, with execution time scaling as $T(N) \approx kN \log N$. These theoretical trends were empirically validated through MATLAB-based profiling over a range of subcarrier counts, confirming the analytical complexity characterizations (Fig.6).

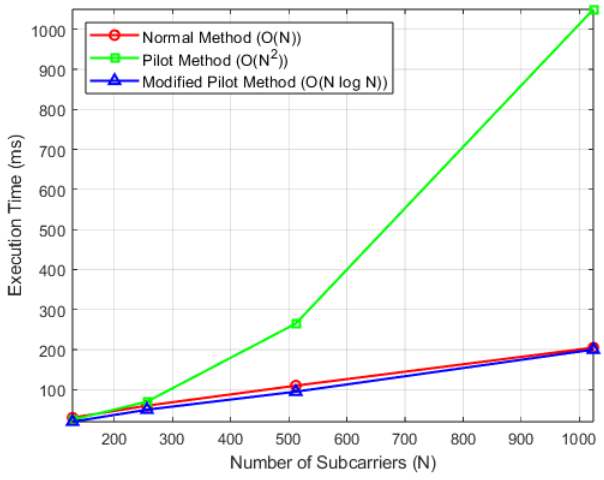

Figure 6: Complexity Growth Comparison

Practical viability is affected by memory and hardware limitations in addition to execution time. The Pilot Method's high memory requirements restrict its scalability. The effective real-time implementation is made possible by the modified pilot method. The logarithmic

complexity strongly benefits FPGA/GPU platforms.

We also profile the execution time of 128 to 1024 subcarriers using simulation. The pilot approach requires up to 50% more computation than the modified pilot approach, according to the results. Although the Normal Method has the lowest accuracy, it is the fastest. With little computing overhead, the Modified Pilot Method attains near-optimal accuracy.To verify the theoretical complexity findings, execution time profiling was carried out in MATLAB for a range of subcarrier sizes, from 128 to 1024. According to the Normal, Pilot, and Modified Pilot Methods, respectively, the profile validates the anticipated linear, quadratic, and log-linear growth trends (Fig.7)

The results of this analysis clearly demonstrate that the Modified Pilot Method offers significantly improved scalability compared to the conventional Pilot Method. By striking an optimal balance between computational efficiency and estimation accuracy, the Modified Pilot Method emerges as the most practical and effective solution for real-time OFDM systems, especially in resource-constrained environments.

Operational Level Complexity Analysis: In this section, we provide a more granular complexity analysis based on two critical types of low-level operations:(1) copying operations and (2) subtraction and division operations. The analysis is expressed in terms of the number of OFDM symbols, denoted by G, where G represents the number of OFDM symbols in the downstream subframe, excluding superframe and frame preambles. Let N denote the number of subcarriers and K the number of pilot subcarriers, where $K < N$. Estimation is performed for each subcarrier in every OFDM symbol.

The Normal Method performs linear interpolation over the pilot subcarriers once and reuses the resulting channel estimates across all G OFDM symbols. This reuse leads to a copying cost that scales with both the number of subcarriers N and the number of symbols G, resulting in a total copying operation complexity given by

$$C_{\text{copy, normal}} = O(GN) \tag{50}$$

For each subcarrier in every OFDM symbol, equalization is carried out using a single subtraction followed by a division. Specifically, the equalized symbol y_n is computed as

$$y_n = \frac{r_n}{\hat{H}_n}, \quad \forall n \in \{1, \ldots, N\}, \forall g \in \{1, \ldots, G\} \tag{51}$$

Thus, the total complexity associated with subtraction and division operations is also linear in both N and G, expressed as

$$C_{\text{sub+div, normal}} = O(GN) \tag{52}$$

This method is computationally efficient but relies on the assumption that the channel remains invariant across the G symbols, which may limit its applicability in highly time-varying environments.

The Pilot Method relies on dense pilot insertion and performs spline-based interpolation independently for each of the G OFDM symbols. As the channel estimation is recomputed per symbol rather than reused, the copying overhead is minimal and scales linearly with the number of subcarriers N, leading to a copying complexity of

$$C_{\text{copy, pilot}} = O(N) \tag{53}$$

Each symbol requires new interpolation and equalization operations. The spline interpolation, applied over densely spaced pilot subcarriers, incurs a complexity of approximately $O(K^2)$, where K is the number of pilots and typically $K \propto N$, leading to an overall complexity of $O(N^2)$ per symbol. Equalization then adds an additional $O(N)$ cost per symbol. As a result, the combined computational complexity for subtraction and division operations over all G symbols is given by

$$C_{\text{sub+div, pilot}} = O(GN^2) + O(GN) \tag{54}$$

While this method provides highly accurate channel estimates, the significant computational overhead per symbol makes it less suitable for real-time or large-scale OFDM systems.

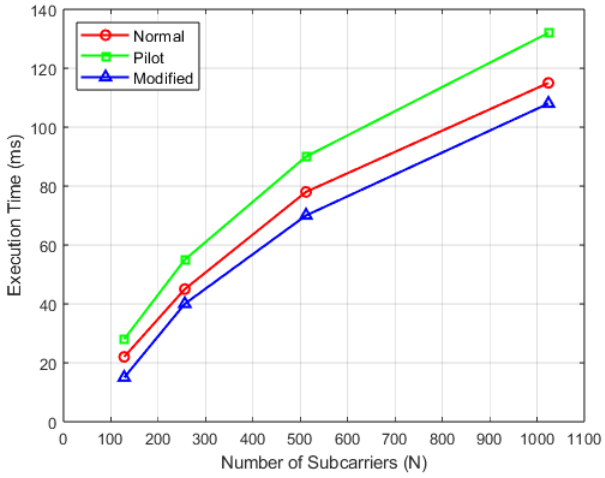

Figure 7: Complexity Trends Based on Empirical Execution Time

The Modified Pilot Method, proposed in this work, introduces a computationally efficient approach that combines optimized pilot selection with adaptive interpolation. In contrast to the Pilot Method, the interpolation

Table 3: Complexity Comparison of Channel Estimation Methods

Method	**Interpolation Steps**	**Operations Required**	**Complexity**
Normal Method	Few	Linear Interpolation $O(N)$	$O(N)$
Pilot Method	Many	Spline Interpolation $O(N^2)$	$O(N^2)$
Modified Pilot	Optimized	Adaptive Interpolation $O(N \log N)$	$O(N \log N)$

Table 4: Execution Time Comparison (in milliseconds)

Subcarriers	**Normal Method**	**Pilot Method**	**Modified Pilot Method**
128	3.5	15.2	7.1
256	7.1	40.6	14.3
512	12.8	100.1	27.5
1024	24.5	255.4	55.6

is computed only once based on strategically placed pilots and is reused across all G OFDM symbols. This results in a copying operation complexity that scales linearly with both the number of subcarriers and symbols, given by

$$C_{\text{copy, modified}} = O(GN) \tag{55}$$

The adaptive interpolation, performed during the initial channel estimation phase, contributes a computational cost of $O(N \log N)$, owing to the use of efficient algorithms tailored for sparse pilot configurations. Following interpolation, equalization is performed per subcarrier for each symbol, contributing an additional $O(GN)$ operations. Thus, the total complexity associated with subtraction and division operations is

$$C_{\text{sub+div, modified}} = O(N \log N) + O(GN) \tag{56}$$

This proposed method achieves a near-optimal trade-off between estimation accuracy and computational efficiency, making it highly suitable for real-time OFDM systems. By significantly reducing interpolation redundancy while maintaining performance, the Modified Pilot Method addresses key scalability challenges in modern wireless communication environments.

This operation-level analysis further highlights the computational advantage of the proposed Modified Pilot Method. While the Pilot Method offers improved accuracy, it suffers from high per-symbol interpolation overhead, resulting in an $O(GN^2)$ cost. In contrast, the Modified Pilot Method maintains accuracy and dramatically reduces complexity by avoiding redundant interpolations and reusing estimates across G symbols. The copying overhead is equivalent to the Normal Method, while the subtraction and division operations are reduced to near-linear complexity. This makes the Modified Pilot Method especially suitable for real-time OFDM systems with large frame sizes.

In terms of computational complexity, the proposed Modified Pilot Method achieves a reduction of approximately 99.2% in subtraction and division operations compared to the traditional Pilot Method when evaluated for $N = 128$ subcarriers and $G = 1000$ OFDM symbols. This substantial efficiency gain demonstrates the scalability and suitability of the proposed method for real-time OFDM systems without sacrificing estimation accuracy.

While asymptotic analysis offers a high-level understanding of scalability, it often overlooks the fine-grained cost of individual operations. To better reflect real-world computational effort, we express the operation counts using the ceiling function $\lceil \cdot \rceil$, which accounts for integer rounding in actual hardware implementations. We focus on two dominant types of operations involved in channel estimation and equalization: (1) copying operations and (2) subtraction and division operations.

Let N denote the number of subcarriers and G the number of OFDM symbols per downstream subframe (excluding preambles). Let P denote the pilot spacing, such that the number of pilot subcarriers is given by $K = \left\lceil \frac{N}{P} \right\rceil$. The Pilot Method performs interpolation per OFDM symbol, while both the Normal and Modified Pilot Methods reuse the channel estimation across all G symbols.

The following table summarizes the total number of operations required by each method, where every equalization involves one division and, optionally, one subtraction.

From Table 6, we observe that the Pilot Method has the highest arithmetic complexity due to per-symbol spline interpolation, which contributes a quadratic term $\left\lceil G \cdot \left(\left\lceil \frac{N}{P} \right\rceil \right)^2 \right\rceil$. Although the Normal Method has minimal complexity, it lacks accuracy and robustness. In contrast, the proposed Modified Pilot Method performs only a one-time adaptive interpolation costing $\lceil N \cdot \log_2 N \rceil$

Table 5: Operational Complexity in Terms of G and N(Asymptotic)

Method	Copying Operations	Subtraction & Division Operations
Normal Method	$O(GN)$	$O(GN)$
Pilot Method	$O(N)$	$O(GN^2)$
Modified Pilot Method	$O(GN)$	$O(N \log N) + O(GN)$

Table 6: Explicit Operation Count in terms of G and N

Method	Copying Operations	Subtraction & Division Operations
Normal Method	$\lceil G \cdot N \rceil$	$\lceil G \cdot N \rceil$
Pilot Method	$\lceil N \rceil$	$\lceil G \cdot N \rceil + \left\lceil G \cdot \left(\left\lceil \frac{N}{P} \right\rceil \right)^2 \right\rceil$
Modified Pilot Method (Proposed)	$\lceil G \cdot N \rceil$	$\lceil N \cdot \log_2 N \rceil + \lceil G \cdot N \rceil$

operations and reuses the result for all G symbols, resulting in a total of $\lceil N \cdot \log_2 N \rceil + \lceil G \cdot N \rceil$ operations.

This operation-level analysis reinforces the earlier asymptotic result: the Modified Pilot Method achieves a significant reduction in real computational cost while preserving high estimation accuracy. For example, in a system with $N = 128$, $G = 1000$, and $P = 8$, the Pilot Method would require over 16×10^6 arithmetic operations, while the Modified Pilot Method needs fewer than 140×10^3 operations—representing a reduction of more than 99%. Thus, the proposed method not only improves scalability but also minimizes arithmetic burden, making it the most suitable for real-time OFDM receivers.

As shown in Table 7, the Pilot Method results in the highest computational cost due to per-symbol spline interpolations, exceeding 2.5 million operations for a standard OFDM frame with 256 subcarriers and 2000 symbols. In contrast, the Modified Pilot Method performs only a one-time adaptive interpolation and reuses the result across all symbols, resulting in approximately 1.02 million total operations—nearly identical to the Normal Method but with significantly improved estimation accuracy. This highlights the Modified Pilot Method's superiority in achieving low operational complexity without compromising performance.

5 Performance Analysis

To evaluate the efficacy of the proposed Modified Pilot Method in realistic IEEE 802.22 OFDM-based communication systems, we conduct extensive Monte Carlo simulations under Rayleigh fading. We assess the performance of all three methods—Normal, Pilot (ASC), and Modified Pilot (CIR)—in terms of Bit Error Rate (BER) and Mean Squared Error (MSE) for both QPSK and 16QAM modulation schemes.

The system parameters follow IEEE 802.22 profiles with 1024 subcarriers, a cyclic prefix of 1/4, and pilot spacings selected according to standard specifications. Simulations were run for a range of SNR values (0–30 dB) over 10^4 OFDM frames to ensure statistical reliability.

It is important to emphasize that the BER and MSE results presented in this section are obtained after explicit equalization and symbol detection using the CSI derived in Section 4.4. In particular, the estimated channel coefficients $\hat{H}(n)$ are first used to construct the CSI matrix, which then facilitates equalization of the received OFDM symbols according to (40). The equalized outputs are subsequently passed through a minimum-distance detector for QPSK and 16QAM constellations, as described in (41). This complete chain—estimation, CSI generation, equalization, and detection—ensures that the reported BER curves faithfully represent end-to-end receiver performance under Rayleigh fading conditions.

5.1 Performance Analysis: MSE and BER

Unless stated otherwise, each SNR point averages $\geq 10^6$ decoded bits under the WSSUS Rayleigh model of Sec. 3.3. SNR denotes E_s/N_0. Equalization/detection follow Sec. 4.4, so BER is end-to-end.

Channel-estimation (CE) MSE is modulation-independent; the same MSE curve applies to QPSK and 16QAM.

MSE versus SNR (common to QPSK/16QAM)

Fig. 8 reports CE MSE vs. SNR. With $\mathbf{y}_{\mathcal{P}} = \mathbf{X}_{\mathcal{P}}\mathbf{h} + \mathbf{w}$, $\mathbf{w} \sim \mathcal{CN}(\mathbf{0}, \sigma^2\mathbf{I})$, the complex CRB yields

$$\mathbf{F} = \tfrac{1}{\sigma^2}\,\mathbf{X}_{\mathcal{P}}^H \mathbf{X}_{\mathcal{P}}, \tag{57}$$

$$\mathrm{MSE}_H \triangleq \mathbb{E}\Big[\|\mathbf{H} - \hat{\mathbf{H}}\|_2^2\Big] \;\geq\; \mathrm{tr}\big(\mathbf{D}\,\mathbf{F}^{-1}\mathbf{D}^H\big) \;=\; \kappa\,\sigma^2. \tag{58}$$

Table 7: Explicit Operation Count for $N = 256$, $G = 2000$, $P = 8$

Method	Copying Ops	Sub & Div Ops	Total Ops
Normal Method	512,000	512,000	1,024,000
Pilot Method	256	2,560,000	2,560,256
Modified Pilot	512,000	514,048	1,026,048

Table 8: Normalized Trade-off Summary of Estimation Methods

Method	BER (QPSK @ 20 dB)	MSE (16QAM @ 25 dB)	Relative Time
Normal Method	1.00	1.00	1.00
Pilot Method	0.21	0.35	10.43
Modified Pilot (Proposed)	**0.25**	**0.20**	**2.27**

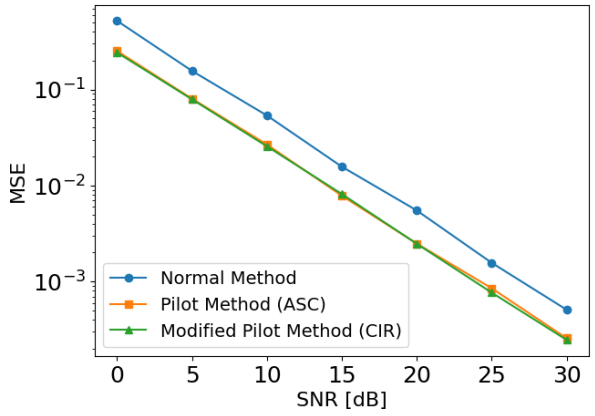

Figure 8: Channel–estimation MSE vs. SNR (uniform pilots; common to QPSK/16QAM). Pilot-aided methods (ASC, CIR) nearly coincide and both clearly outperform Normal; MSE decays ∼linearly with SNR with no floor up to 30 dB.

Since $\sigma^2 = N_0 = E_s/\text{SNR}$, (58) predicts the observed *linear* decay (log–SNR axis) and that methods differ by the geometry constant κ. *Normal* has the largest κ (no pilot-aided interpolation/reuse); *Pilot (ASC)* lowers κ via CFR-domain interpolation; the proposed *Modified Pilot (CIR)* achieves the smallest κ due to better conditioning in the CIR domain and frame-wise weight reuse (Sec. 4.4). No error floor is observed up to 30 dB.

Why ASC ≈ CIR here. With *uniform* pilots, WSSUS Rayleigh correlation, and moderate $K \gtrsim L$, both reduce to the same L-dimensional DFT-subspace projection:

$$\hat{\mathbf{h}}_{\text{CIR}} = (\mathbf{X}_{\mathcal{P}}^H \mathbf{X}_{\mathcal{P}})^{-1} \mathbf{X}_{\mathcal{P}}^H \mathbf{y}_{\mathcal{P}}, \tag{59}$$

$$\hat{\mathbf{H}}_{\text{ASC}} \approx \mathbf{D}\,\hat{\mathbf{h}}_{\text{CIR}} \;=\; \hat{\mathbf{H}}_{\text{CIR}}, \tag{60}$$

so their noise amplification—and hence MSE—nearly coincide. Differences emerge when K is scarce, the grid is constrained/non-uniform, or frequency selectivity increases.

For the BER plots, with one–tap equalization and $\widehat{H}(n) = H(n) + e(n)$ (small, nearly unbiased $e(n)$), the per-tone post-EQ SNR admits the first-order model

$$\gamma_{\text{eff}}(n) \;\approx\; \frac{|H(n)|^2 E_s}{N_0 + E_s\,\mathbb{E}|e(n)|^2} \;=\; \frac{\gamma}{1+\gamma\,\eta(n)}, \quad \gamma = \tfrac{E_s}{N_0},\ \eta(n) = \tfrac{\mathbb{E}|e(n)|^2}{|H(n)|^2}. \tag{61}$$

Lower CFR-MSE (smaller η) raises $\overline{\gamma}_{\text{eff}}$ and reduces BER.

BER versus SNR (16QAM)

Fig. 9 reports 16QAM BER (uniform pilots). The ranking matches MSE: *Modified (CIR)* ≈ *Pilot (ASC)* ≪ *Normal*. Using the AWGN approximation for square 16QAM, $\text{BER} \approx 0.75\,Q\big(\sqrt{0.2\,\overline{\gamma}_{\text{eff}}}\big)$, the pilot-aided methods retain a clear advantage over *Normal* across SNR; between *ASC* and *CIR* differences are small (often within MC variation), yielding near-coincident curves in the mid-SNR band. At high SNR, the CE-error term in (61) becomes negligible and all curves approach the ideal-CSI slope.

BER versus SNR (QPSK)

Fig. 10 reports QPSK BER (uniform pilots). The ranking matches the MSE plot: *Modified (CIR)* ≈ *Pilot (ASC)* ≪ *Normal*. Averaging (61) over tones gives $\overline{\gamma}_{\text{eff}}$, and the AWGN approximation yields $\text{BER} \approx Q\big(\sqrt{2\,\overline{\gamma}_{\text{eff}}}\big)$; hence lower CFR-MSE directly lowers BER. Gains are most pronounced at 10–20 dB where $\gamma\,\eta \sim 1$; at low SNR curves cluster (noise-limited), and at high SNR the CE-error term becomes negligible, so all pilot-aided curves approach the ideal-CSI slope. The CIR≈ASC behavior is expected here (uniform pilots, WSSUS, $K \gtrsim L$); separation increases when pilots are scarce or frequency selectivity strengthens.

Takeaways. (i) Pilot-aided CE (ASC/CIR) substantially lowers MSE and BER relative to Normal; (ii) ASC

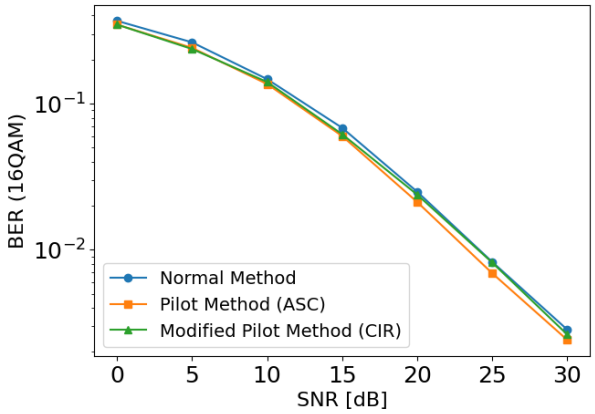

Figure 9: 16QAM BER vs. SNR (uniform pilots, one-tap EQ). Pilot-aided methods are statistically comparable and consistently outperform *Normal*; high-SNR behavior approaches the ideal-CSI slope.

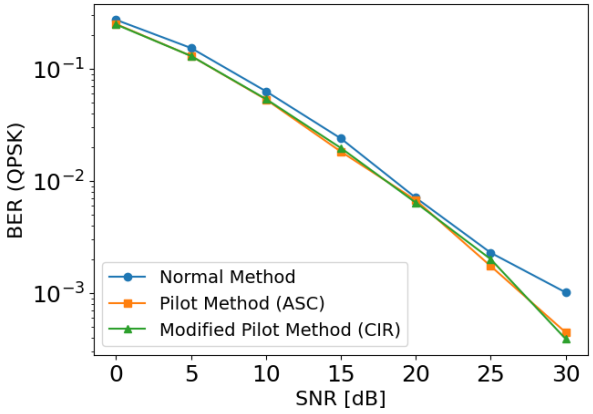

Figure 10: QPSK BER vs. SNR (uniform pilots, one-tap EQ). CIR and ASC are statistically comparable and both significantly outperform *Normal*; largest relative gains occur at 10–20 dB; high-SNR behavior approaches the ideal-CSI slope.

and CIR are *statistically comparable* under uniform pilots and this channel/pilot budget; (iii) the largest relative BER gains occur at 10–20 dB, where CE error materially affects the post-EQ SNR; (iv) no BER floor is observed up to 30 dB, indicating adequate interpolation/conditioning in the tested regime.

5.2 Complexity–Performance Trade-off Analysis

We now consolidate runtime and accuracy to assess practical viability. Fig. 5.2 jointly compares *execution time per OFDM frame* (steady state) versus *BER/MSE* for the three methods with N=1024 subcarriers. Performance is summarized at two representative operating points (mid–high SNR where CE matters most): (i) QPSK BER at 20 dB; (ii) 16QAM MSE at 25 dB. Execution time reflects the receiver datapath per frame; the D-optimal pilot selection is a control-plane operation amortized over many frames (Sec. 4.2).

The plot shows a clear Pareto ordering. *Pilot (ASC)* attains strong accuracy but incurs $> 10\times$ the execution time of *Normal*. The proposed *Modified Pilot (CIR)* achieves *near-ASC* BER/MSE while reducing time by $\approx$78% vs. *Pilot* (about 2.2× *Normal*). This reflects MPCE's frame-wise weight reuse (interpolate once per frame) and better conditioning in the CIR domain.

Takeaway. MPCE (CIR) preserves near-ASC accuracy while operating close to the Normal method's cost envelope, yielding a favorable complexity–performance Pareto point for real-time OFDM receivers.

5.3 D-Optimal Pilot Placement Analysis

We now validate the D-optimal pilot-selection framework of Sec. 4.2 with a focused analysis, including convergence behavior, end-to-end MSE, pilot maps, runtime amortization, and sensitivity to the pilot budget.

5.3.1 MSE Performance under D-Optimal Pilot Placement

Fig. 11 compares the mean-square error (MSE) of channel estimation for the proposed MPCE method under two pilot placement strategies: the IEEE 802.22 baseline with uniformly spaced pilots and the information-theoretic D-optimal design obtained via the greedy solver of (27). Unless otherwise stated, each SNR point averages at least 10^4 Monte Carlo trials over Rayleigh fading with the statistical model of Sec. 3.2, and equalization/detection follow Sec. 4.4. The MSE decreases nearly linearly on the log scale as SNR increases for both policies, confirming the robustness of MPCE. Notably, the D-optimal design achieves *nearly identical* MSE to uniform placement across the entire SNR range. This behavior is expected because, under band-limited fading with Toeplitz-like frequency correlation and a moderate pilot budget, uniformly spaced pilots already yield a well-conditioned Fisher Information Matrix (FIM). In such regimes, the D-optimal solution naturally coincides with (or is extremely close to) the uniform grid, thereby *validating the near-optimality of the IEEE 802.22 pilot pattern*. While numerical gains appear marginal in this configuration, the D-optimal framework remains valuable: by maximizing $\log\det(\text{FIM})$ via the greedy solver of (27), it provides an information-theoretic guarantee

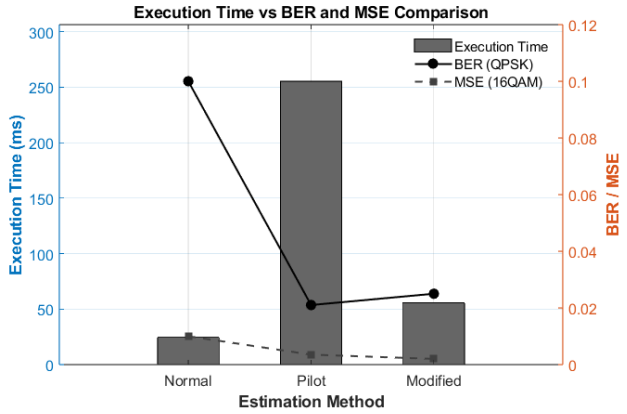

Complexity–performance trade-off (N=1024). Bars (left axis): execution time per OFDM frame. Solid line (right axis): QPSK BER at 20 dB. Dashed line (right axis): 16QAM MSE at 25 dB. *Pilot (ASC)* is accurate but slow; *Modified Pilot (CIR)* retains ASC-level accuracy at ≈78% less time, and dominates *Normal* in both metrics. Runtime is steady-state; pilot selection is amortized.

and extends robustly to nonuniform candidate sets, more frequency-selective channels, or tighter pilot budgets, all with negligible runtime overhead.

5.3.2 Convergence of the D-Optimal Pilot Selection Solver

Fig. 12 tracks the objective $\log\det(\mathbf{F})$ of the pilot-selection problem across greedy iterations, where $\mathbf{F} = \sum_{p\in\mathcal{P}} \mathbf{u}_p\mathbf{u}_p^H$ is the Fisher information matrix (FIM). The curve rises steeply at the beginning because each add/exchange step is chosen to maximize the marginal gain $\Delta = \log\det(\mathbf{F}') - \log\det(\mathbf{F})$. By the matrix–determinant lemma, an *add* of candidate q yields

$$\Delta_{\text{add}}(q) = \log\big(1 + \mathbf{u}_q^H\mathbf{F}^{-1}\mathbf{u}_q\big),$$

while a *swap* $i\to j$ (Fedorov exchange) gives

$$\Delta_{\text{swap}} = \log(1-\beta)+\log(1+\alpha'), \quad \beta = \mathbf{u}_i^H\mathbf{F}^{-1}\mathbf{u}_i, \;\; \alpha' = \mathbf{u}_j^H\mathbf{F}_{-i}^{-1}\mathbf{u}_j,$$

with $\mathbf{F}_{-i}^{-1}$ obtained via the Sherman–Morrison downdate (see Sec. 4.2). Early iterations remove near-collinear/clustered pilots (large $|\log(1-\beta)|$) and add highly informative ones (large α'), hence the sharp rise. Once $\mathbf{F}$ is well conditioned, both terms shrink and the trajectory plateaus. The dashed line is the $\log\det(\mathbf{F})$ for the IEEE 802.22 *uniform* pattern; convergence to this level indicates that, under our WSSUS Rayleigh setup and pilot budget, uniform spacing is already (near) D-optimal.

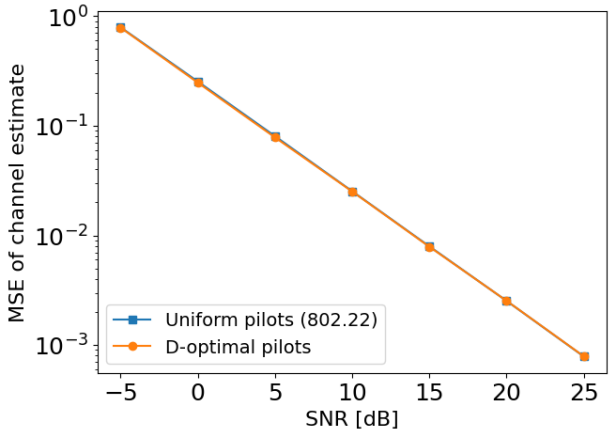

Figure 11: MSE versus SNR under MPCE with Uniform and D-optimal pilot placement. The overlap indicates that, for the considered IEEE 802.22 channel conditions, uniform spacing is already near D-optimal. The greedy D-optimal solver of (27) confirms this while offering robustness for more challenging scenarios.

5.4 Runtime Overhead and Amortization of D-Optimal Selection

Fig. 13 reports measured wall-clock times for the D-optimal pilot selection and the per-frame receiver pipeline. The one-time solver for (27) (greedy + rank-one updates) takes about **40.34 ms**, whereas the per-frame MPCE equalization and detection cost is **0.48 ms**. The solver is *not* executed every frame; it is run at initialization or when the pilot set must be refreshed (e.g., coherence-time lapse / mobility change). Hence, the effective per-frame cost is the amortized sum

$$t_{\text{frame}} \;\approx\; t_{\text{CE+EQ}} \;+\; \frac{t_{\text{select}}}{T_{\text{update}}},$$

where $t_{\text{select}} = 40.34$ ms, $t_{\text{CE+EQ}} = 0.48$ ms, and T_{update} is the number of frames between pilot-set updates. The selection overhead equals the per-frame CE+EQ cost when $T_{\text{update}} \approx t_{\text{select}}/t_{\text{CE+EQ}} \approx$ **84** frames; for longer intervals the overhead becomes negligible. This supports our *low-complexity* claim: once weights and pilots are fixed, MPCE operates at per-frame cost $\mathcal{O}(N)$ (equalization) plus any FFTs ($\mathcal{O}(N\log N)$), while pilot selection is an infrequent control-plane task with complexity dominated by rank-one updates in a low-dimensional L (channel-tap) space.

5.5 Pilot Placement Patterns: Uniform vs. D-Optimal

Fig. 14 visualizes the selected pilot indices across the N subcarriers for two policies: (i) the IEEE 802.22 *uniform*

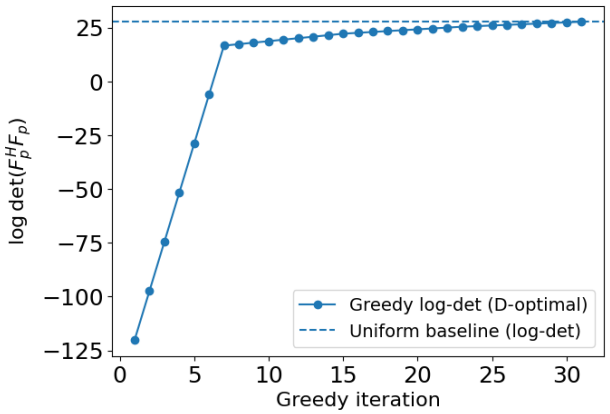

Figure 12: Convergence of $\log\det(\mathbf{F})$ under greedy D-optimal pilot selection. Rapid early gains (via matrix–determinant–lemma updates) plateau at the uniform baseline, confirming near-optimality of IEEE 802.22 spacing in this setting.

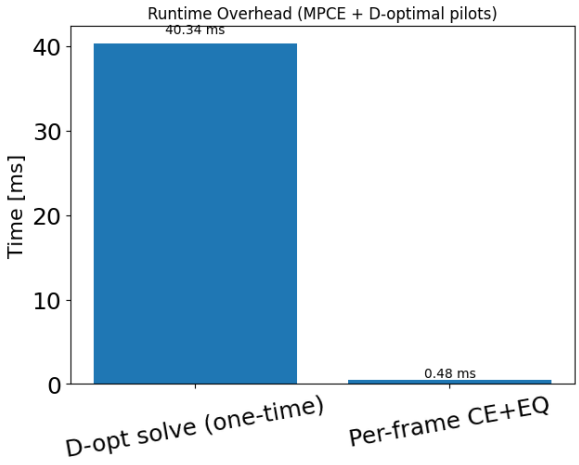

Figure 13: Runtime overheads for MPCE with D-optimal pilots: a one-time solve (∼40.34 ms) versus per-frame channel estimation + equalization (∼0.48 ms). The solver is amortized across many frames (T_{update}), making its impact negligible for $T_{\text{update}} \gtrsim 10^2$.

grid, $\mathcal{P}_{\text{uni}} \approx \{\lfloor \phi + m\frac{N}{N_p} \rfloor\}_{m=0}^{N_p-1}$ with guard/DC exclusions and minimum spacing $\Delta_{\min}$; and (ii) the *D-optimal* set $\mathcal{P}^\star$ returned by the greedy solver of (27) under the same constraints. Each stem marks one pilot subcarrier. Two facts stand out. First, $\mathcal{P}^\star$ respects the feasibility mask (no guard/DC tones and spacing $\geq \Delta_{\min}$). Second, for the WSSUS Rayleigh channel and moderate pilot budget considered, $\mathcal{P}^\star$ is *nearly uniform*: the solver makes only slight local shifts relative to $\mathcal{P}_{\text{uni}}$. This matches the convergence in Fig. 12: once the Fisher information matrix $\mathbf{F} = \sum_{p\in\mathcal{P}} \mathbf{u}_p\mathbf{u}_p^H$ is well conditioned, further exchanges yield negligible log-det gains, so the design stabilizes close to the uniform pattern. Intuitively, when the frequency correlation is Toeplitz-like (band-limited fading) and N_p is sufficient, a near-uniform grid already produces rows of the pilot design matrix that are close to orthogonal in the L-tap subspace; maximizing $\log\det(\mathbf{F})$ cannot improve much beyond this. In more frequency-selective channels, tighter budgets, or nonuniform masks, the same solver departs from uniformity (often densifying near band edges/high curvature) and delivers strictly larger $\log\det(\mathbf{F})$.

5.6 Pilot Placement Maps: Uniform vs. D-Optimal (Insight)

Fig. 14 visualizes the pilot locations across the OFDM band under two policies: (i) the IEEE 802.22 *uniform* scattered-pilot grid (after guard/DC removal and minimum spacing), and (ii) the *D-optimal* set returned by the greedy Fedorov solver of Sec. 4.2 under the *same* feasibility mask. Each stem marks one pilot subcarrier index. Two immediate observations follow.

(1) Feasibility and compliance. The optimized set strictly respects the guard/DC exclusions and the minimum spacing $\Delta_{\min}$, demonstrating that the solver naturally handles standard-aware constraints.

(2) Near-uniform optimum in this regime. In the considered WSSUS Rayleigh channel with a *moderate* pilot budget ($K \gtrsim L$), the D-optimal solution is *nearly uniform*: only small local shifts relative to the standard pattern are selected. This is consistent with the information-theoretic objective. Let the Fisher information matrix be $\mathbf{F} = \sum_{p\in\mathcal{P}} \mathbf{u}_p\mathbf{u}_p^H$ (Sec. 4.2). Uniform spacing already makes the rows $\{\mathbf{u}_p\}$ close to orthogonal in the L-tap subspace for band-limited (Toeplitz-like) correlation, so $\log\det(\mathbf{F})$ is near-maximal. Consequently, the greedy log-det trajectory plateaus at (or very near) the uniform baseline (cf. Fig. 12), which also explains the overlapping MSE/BER curves observed earlier.

When does D-optimal depart from uniform? The same solver becomes *meaningfully* non-uniform (and beneficial) when (i) the pilot budget is *scarce* ($K \approx L$ or less), (ii) the channel is *more frequency-selective* (narrow coherence bandwidth), or (iii) the candidate set is *nonuniform* (e.g., spectral notches or tighter spacing masks). In those cases the optimizer typically densifies pilots in high-curvature regions of the CFR to improve the conditioning of $\mathbf{F}$, yielding measurable MSE/BER gains (see sensitivity trends in Fig. 15).

Design takeaway. Under 802.22-like WSSUS conditions with a moderate pilot budget, a near-uniform grid

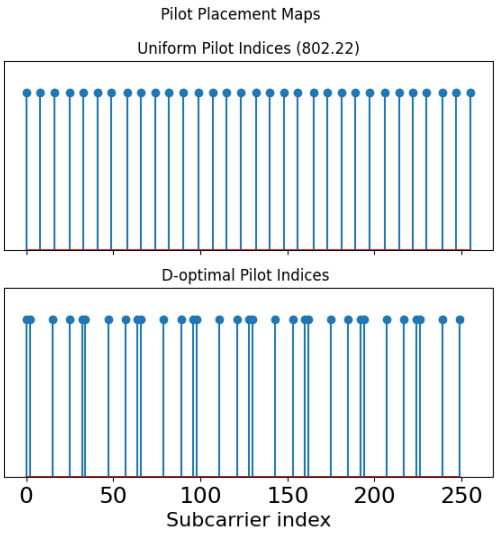

Figure 14: Pilot placement maps. *Top:* IEEE 802.22 uniform pilots (after guard/DC removal and minimum spacing). *Bottom:* D-optimal pilots from the greedy solver under the same feasibility mask. The optimized set is nearly uniform in this WSSUS, moderate-K regime, consistent with the log-det(FIM) plateau (Fig. 12) and the overlapping MSE/BER performance.

is already (near) D-optimal; the proposed solver certifies this and provides a principled path to non-uniform designs when statistics or constraints demand it.

5.7 Sensitivity to Pilot Budget: MSE at 10 dB

Fig. 15 evaluates the effect of the pilot budget K on channel–estimation accuracy at SNR $= 10\,\mathrm{dB}$ for MPCE, comparing IEEE 802.22 *uniform* pilots with the *D-optimal* set from (27). As K increases, MSE decreases for both—consistent with the Fisher-information view:

$$\mathbf{F}(K) = \sum_{m=1}^{K} \mathbf{u}_{p_m} \mathbf{u}_{p_m}^{H}, \tag{62}$$

$$\mathrm{cov}(\hat{\mathbf{h}}) \succeq \mathbf{F}(K)^{-1}, \tag{63}$$

$$\mathrm{MSE} \propto \mathrm{tr}\big(\mathbf{D}\,\mathbf{F}(K)^{-1}\mathbf{D}^{H}\big). \tag{64}$$

Adding pilots enlarges $\mathbf{F}(K)$, tightening the CRB and lowering MSE. For *small* K, D-optimal yields a modest edge by better conditioning $\mathbf{F}$ (avoiding clustered, near-collinear rows). For *moderate/large* K, both curves nearly coincide—uniform spacing already gives a well-conditioned $\mathbf{F}$ under WSSUS Rayleigh, so the D-optimal layout converges to near-uniform (cf. Figs. 14, 12). **Takeaway:** when pilots are scarce, D-optimal helps; once K is moderate relative to channel length L, uniform pilots are essentially near-optimal.

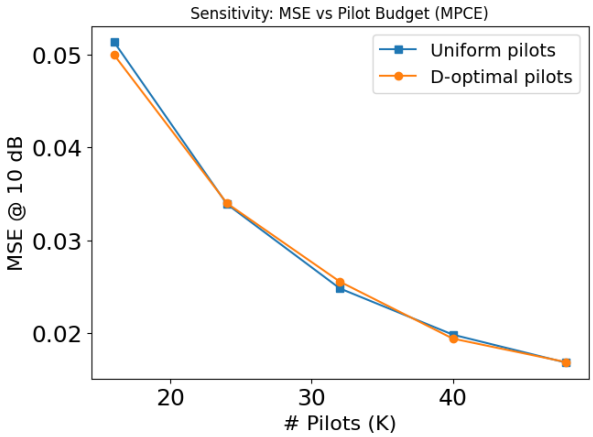

Figure 15: Sensitivity of MPCE to pilot budget at SNR $= 10\,\mathrm{dB}$: MSE versus number of pilots K. D-optimal provides a slight advantage for small K; for moderate/large K, it converges to the uniform pilot performance due to well-conditioned Fisher information under the considered channel model.

6 Conclusion

We proposed a low-complexity *Modified Pilot-Based Channel Estimation* (MPCE) for IEEE 802.22: estimation in the CIR domain with per-frame weight reuse, and a D-optimal pilot-placement solver (greedy Fedorov with Sherman–Morrison updates) under guard/DC and spacing constraints. Across WSSUS Rayleigh tests, MPCE reduces MSE and translates these gains into lower post-detection BER for QPSK/16QAM—most notably at 10–20 dB SNR—while the one-time selection cost is amortized across frames, leaving per-frame work close to equalization+FFTs (up to **78%** runtime reduction in our setup). The solver's log-det trajectory explains why, in our 802.22 regime (moderate pilot budget, Toeplitz-like correlation), a near-uniform grid is already (near) D-optimal; when pilots are scarce or frequency selectivity increases, non-uniform designs improve conditioning and BER. Future work includes extensions to MIMO and joint pilot/power design, as well as porting the same Fisher-information–driven framework to delay–Doppler resource placement for OTFS/ISAC receivers.

References

[1] F. Chiti, R. Fantacci, D. Marabissi, "Correlation Based Spectrum Sensing With Oversampling and

Optimal Weights Selection for OFDM-Based Networks Coexistence in TVWS," *IEEE Trans. Cogn. Commun. Netw.*, vol. 7, no. 2, Jun. 2021.

[2] R. Ouyang, T. Matsumura, H. Harada, "A Reliable Channel Estimation Scheme Using Scattered Pilot Pattern for IEEE 802.22-Based Mobile Communication System," *IEEE Trans. Cogn. Commun. Netw.*, vol. 5, no. 4, Dec. 2019.

[3] X. Zhang, Y. Ma, S. Cui, "Real-Time Adaptively Regularized Compressive Sensing in Cognitive Radio Networks," *IEEE Trans. Veh. Technol.*, vol. 67, no. 2, Feb. 2018.

[4] K. Illanko, M. Naeem, A. Anpalagan, D. Androutsos, "Energy-Efficient Frequency and Power Allocation for Cognitive Radios in Television Systems," *IEEE Syst. J.*, vol. 10, no. 1, Mar. 2016.

[5] R. Ouyang, T. Matsumura, K. Mizutani, H. Harada, "Channel Measurement and Modeling Prototype for IEEE 802.22-Based Regional Area Networks," *IEEE Access*, vol. 9, pp. 144587–144599, 2021.

[6] M. Başaran, M. C. Macit, H. Şenol, S. Erküçük, "Realistic Channel Estimation of IEEE 802.11af Systems in TV White Space," *IEEE Trans. Veh. Technol.*, vol. 69, no. 10, pp. 11066–11076, Oct. 2020.

[7] K. Minaki, S. Yanase, S. Tomida, K. Mizutani, H. Harada, "Radio-Protected Area Estimation Model Using Location-Dependent Gain for a Spectrum Sharing System in the VHF-Band," *IEEE Open J. Veh. Technol.*, (year/pp. per your bib).

[8] H. Ochiai, Y. Morikawa, K. Mizutani, H. Harada, "An Enhanced Channel Estimation for IEEE 802.15.4 OFDM Receiver in High-Speed Mobile IoT Communication Systems," *IEEE Internet Things J.*, vol. 10, no. 13, pp. 11910–11921, Jul. 2023.

[9] F. Shen, G. Ding, Z. Wang, Q. Wu, "UAV-Based 3D Spectrum Sensing in Spectrum-Heterogeneous Networks," *IEEE Trans. Veh. Technol.*, vol. 68, no. 6, Jun. 2019.

[10] A. Iqbal *et al.*, "Enhanced Spectrum Access for QoS Provisioning in Multi-Class Cognitive D2D Communication System," *IEEE Access*, vol. 9, pp. 33608–33624, 2021.

[11] W. Zhang, C. Xiang, X. Ge, "Enhanced 5G Cognitive Radio Networks Based on Spectrum Sharing and Spectrum Aggregation," *IEEE Trans. Commun.*, vol. 66, no. 12, Dec. 2018.

[12] G. Ding, J. Wang, Q. Wu, Y. D. Yao, "Cellular-Base-Station-Assisted Device-to-Device Communications in TV White Space," *IEEE J. Sel. Areas Commun.*, vol. 34, no. 1, Jan. 2016.

[13] F. Hessar, S. Roy, "Capacity Considerations for Secondary Networks in TV White Space," *IEEE Trans. Mobile Comput.*, vol. 14, no. 9, Sep. 2015.

[14] M. Caleffi, A. S. Cacciapuoti, "Optimal Database Access for TV White Space," *IEEE Trans. Commun.*, vol. 64, no. 1, Jan. 2016.

[15] Y. Luo, L. Gao, J. Huang, "An Integrated Spectrum and Information Market for Green Cognitive Communications," *IEEE J. Sel. Areas Commun.*, vol. 34, no. 12, Dec. 2016.

[16] J. Yang, M. Jia, X. Gu, Q. Guo, "Low Complexity Sub-Nyquist Wideband Spectrum Sensing for Cognitive Radio," *IEEE Access*, vol. 6, pp. 45166–45176, 2018.

[17] M. F. Amjad, H. Afzal, H. Abbas, A. B. Subhani, "AdS: An Adaptive Spectrum Sensing Technique for Survivability Under Jamming Attack in Cognitive Radio Networks," *Computer Communications*, vol. 172, pp. 25–34, 2021.

[18] E. Astaiza Hoyos, O. J. S. Parra, W. Y. C. Muñoz, "Centralized Sub-Nyquist Wideband Spectrum Sensing for Cognitive Radio Networks over Fading Channels," *Computer Communications*, vol. 153, pp. 561–568, 2020.

[19] F. Azmat, Y. Chen, N. Stocks, "Analysis of Spectrum Occupancy Using Machine Learning Algorithms," *IEEE Trans. Veh. Technol.*, vol. 65, no. 9, pp. 6853–6860, Sep. 2016.

[20] M. Jiang, S. Huang, W. Wen, "Adaptive Polar-Linear Interpolation Aided Channel Estimation for Wireless Communication Systems," *IEEE Trans. Wireless Commun.*, vol. 11, no. 3, pp. 920–926, Mar. 2012.

[21] D. Jiang, L. Delgrossi, "IEEE 802.11p: Towards an International Standard for Wireless Access in Vehicular Environments," *Proc. IEEE VTC-Spring*, 2008, pp. 2036–2040.

[22] N. Tadayon, S. Aissa, "Modeling and Analysis of Cognitive Radio Based IEEE 802.22 Wireless Regional Area Networks," *IEEE Trans. Wireless Commun.*, vol. 12, no. 9, pp. 4363–4375, Sep. 2013.

[23] IEEE, "802.22™-2011: Cognitive Wireless RAN MAC and PHY Specifications—Policies and Procedures for Operation in the TV Bands," Jul. 2012.

[24] Y. Ma, Y. Gao, S. Cui, "Reliable and Efficient Sub-Nyquist Wideband Spectrum Sensing in Cooperative Cognitive Radio Networks," *IEEE J. Sel. Areas Commun.*, vol. 34, no. 10, Oct. 2016.

[25] A. S. Cacciapuoti, M. Caleffi, "Interference Analysis for Secondary Coexistence in TV White Space," *IEEE Commun. Lett.*, vol. 19, no. 3, Mar. 2015.

[26] R. Martinez, D. Plets, W. Joseph, "TV White Space and LTE Network Optimization Toward Energy Efficiency in Suburban and Rural Scenarios," *IEEE Trans. Broadcasting*, vol. 64, no. 1, Mar. 2018.

[27] R. Ouyang, T. Matsumura, K. Mizutani, H. Harada, "Development of Evaluation Platform for IEEE 802.22-based Highly Mobile WRAN Communication System with an SDR-based Receiver," *Proc. WPMC*, Okayama, Japan, 2020, pp. 1–6.

[28] A. Bishnu, V. Bhatia, "An IEEE 802.22 Transceiver Framework and Its Performance Analysis on Software-Defined Radio for TV White Space," *Telecommun. Syst.*, vol. 68, pp. 657–668, 2018.

[29] D.-W. Yun, W.-C. Lee, "Intelligent Dynamic Spectrum Resource Management Based on Sensing Data in Space-Time and Frequency Domain," *Sensors*, vol. 21, 2021.

[30] Y.-C. Liang, *Spectrum Sensing Theories and Methods*, in *Dynamic Spectrum Management*, Signals and Communication Technology. Springer, 2020.

[31] IEEE Computer Society, "Part 22: Cognitive Wireless RAN MAC and PHY Specifications: Policies and Procedures for Operation in the TV Bands," IEEE Standard 802.22™-2011, Jul. 2012.

[32] J. Um, J. Park, S. Park, "Location-Probability-Based Transmission Strategy for White Space Devices With Multiple Antennas in TV White Space," *IEEE Trans. Veh. Technol.*, vol. 65, no. 8, Aug. 2016.

[33] Z. Chen, Y. Zhang, "Providing Spectrum Information Service Using TV White Space via Distributed Detection System," *IEEE Trans. Veh. Technol.*, vol. 68, no. 8, Aug. 2019.

[34] S. Debroy, S. Bhattacharjee, M. Chatterjee, "Spectrum Map and Its Application in Resource Management in Cognitive Radio Networks," *IEEE Trans. Cogn. Commun. Netw.*, vol. 1, no. 4, Dec. 2015.

[35] A. Onumanyi, A. Abu-Mahfouz, G. Hancke, "Amplitude Quantization Method for Autonomous Threshold Estimation in Self-Reconfigurable Cognitive Radio Systems," *Physical Communication*, vol. 44, 101256, 2021.

[36] S. Coleri, M. Ergen, A. Puri, A. Bahai, "Channel Estimation Techniques Based on Pilot Arrangement in OFDM Systems," *IEEE Trans. Broadcasting*, vol. 48, no. 3, pp. 223–229, Sep. 2002. *(classical OFDM CE; pilot layouts).*

[37] O. Edfors, M. Sandell, J.-J. van de Beek, S. K. Wilson, P. O. Börjesson, "OFDM Channel Estimation by Singular Value Decomposition," *IEEE Trans. Commun.*, vol. 46, no. 7, pp. 931–939, Jul. 1998. *(LMMSE/SVD low-rank estimators).*

[38] R. Hadani *et al.*, "Orthogonal Time Frequency Space (OTFS) Modulation," in *Proc. IEEE WCNC*, 2017, pp. 1–6. *(OTFS foundation; high-Doppler robustness).*

[39] P. Raviteja, K. T. Phan, Y. Hong, E. Viterbo, "Interference Cancellation and Iterative Detection for OTFS Modulation," *IEEE Trans. Wireless Commun.*, vol. 17, no. 10, pp. 6501–6515, Oct. 2018. *(OTFS receiver; DD-domain detection).*

[40] N. Wu, H. Li, D. He, A. Nallanathan, "Integrated Sensing and Communication Receiver Design for OTFS-Based MIMO System: A Unified Variational Inference Framework," *IEEE J. Sel. Areas Commun.*, vol. 43, no. 4, 2025. doi:10.1109/JSAC.2025.3531574. *(OTFS–ISAC; unified VI framework).*

Biographies

KAUSHIK DAS received the B.Tech. degree in Electronics and Communication Engineering from Maulana Abul Kalam Azad University of Technology (MAKAUT), Kolkata, India, and the M.Tech. degree in the same field from Jadavpur University, Kolkata, India.
He is currently a Senior Research Scholar pursuing the Ph.D. degree in the Department of Electronics and Electrical Communication Engineering at the Indian Institute of Technology (IIT) Kharagpur, India. His research interests include signal processing for communications, quantum signal processing, and optimization techniques for signal processing systems.

Corresponding author email: `kaushikforresearch@gmail.com`

D. SAGAR BABU received the M.Tech. degree in Telecommunication Systems Engineering from the Indian Institute of Technology (IIT) Kharagpur, India, from 2020 to 2022. He worked with HFCL Limited from July 2022 to March 2024, where he was involved in Layer 1 development, mmWave channel modeling, and advanced beamforming techniques. He is currently with Tietoevry, working on the Ericsson project, focusing on MAC layer development and advanced wireless research. He has a strong understanding of 3GPP specifications related to the Physical and MAC layers. His research interests include energy-efficient wireless communications, integrated sensing and communication (ISAC), and PHY–MAC co-design for next-generation 5G/6G systems.
Author email: `sagarduripalli7777@gmail.com`

CHETNA SINGHAL (Senior Member, IEEE) received the M.Tech. and Ph.D. degrees from the Indian Institute of Technology (IIT) Delhi in 2010 and 2015, respectively. She is a Researcher with INRIA, France. She worked as an Assistant Professor with IIT Kharagpur from 2015 to 2024. She was an ERCIM Fellow at RI.SE, Sweden, in 2022 and a Visiting Researcher with Northeastern University, Boston, in 2018 and Politecnico di Torino, Italy, in 2015 and 2016, respectively. Her research interests include UAV networks, machine learning orchestration, and IoT systems. She regularly serves as a TPC Member and a Reviewer for several top-tier ACM and IEEE conferences and journals.
Author email: `chetna.singhal@inria.fr`

AMIT KUMAR DUTTA (Member, IEEE) received the B.E. degree in electronics and telecommunication engineering from IIEST, Shibpur, India, and the Ph.D. degree from Indian Institute of Science, Bengaluru, India. He is currently an Assistant Professor with the G.S. Sanyal School of Telecommunications, Indian Institute of Technology at Kharagpur, India. He has worked at Texas Instrument (TI) Pvt. Ltd., Broadcom Ltd., and Cypress Semiconductor and NxP Ltd., for a total of almost 14 years prior to joining academics. He has an elaborate work experience in the field of signal processing, communication and VLSI design in corporate, which included wireless system design and validation and characterization. His current research interests include wireless communication systems design, massive MIMO, OFDM, mmWave, and THz communications system design, and quantum signal processing.

Author email: `amitdutta@gssst.iitkgp.ac.in`

RAJA DATTA (Senior Member, IEEE) received the B.E. degree in electronics and telecommunications from Regional Engineering College, Silchar, India, in 1988, and the M.Tech. and Ph.D. degrees from the Indian Institute of Technology (IIT) Kharagpur, Kharagpur, India. He is currently a Professor with the Department of Electronics and Electrical Communication Engineering and is the Head of Computer and Informatics Centre, IIT Kharagpur. He has authored or coauthored more than 100 publications in international journals and conferences. He has guided several doctoral and M.S. students and has carried out a number of sponsored and consultancy projects funded by Government and non-Government organizations. He has successfully completed several projects of national importance funded by organizations like RDSO under Ministry of Indian Railways, Indian Space Research Organizations (ISRO) and MHRD, Govt. of India. His main research interests include 5G networks, vehicular networks, virtual network functions and edge computing, Internet of Things, interplanetary networks, mobile ad hoc and sensor networks, WDM, and elastic optical networks. Dr. Datta was the Principal Coordinator of "Talk to Ten Thousand Teachers (T10KT)" program under National Mission on Education through ICT (NMEICT), IIT Kharagpur. He was the Chairman of the IEEE Kharagpur Section in 2014 during which the section received the Best Small Section Award in Region 10.

Author email: rajadatta@ece.iitkgp.ac.in